



Original Paper

# 3D Static Modeling and Petrographic Aspects of the Albian/Cenomanian Reservoir, Komombo Basin, Upper Egypt

Moamen Ali <sup>1,4</sup>, A. Abdelhady,<sup>2</sup> Ahmed Abdelmaksoud,<sup>1</sup> M. Darwish,<sup>3</sup> and M. A. Essa<sup>1</sup>

Received 17 May 2019; accepted 10 July 2019

Published online: 17 July 2019

The Albian/Cenomanian reservoir is one of the two main reservoirs composing the petroleum system in the Komombo Basin. However, these reservoirs have not previously been studied in detail. Therefore, a detailed study of the reservoirs is performed. Six boreholes, three vertical seismic profiles and twenty 2D seismic lines are integrated in the Petrel™ Schlumberger modeling software to build a 3D structural model for the Albian/Cenomanian reservoir. This model represents a framework for the subsequent 3D facies and petrophysical models of the studied reservoir. The interpretation of the created maps and 3D models shows two normal fault directions: NW–SE and NE–SW, where the NW–SE direction is dominant, creating a major half-graben system. Conventional well log analyses are performed for the available wells. The results are used in subsequent facies and petrophysical modeling. The thickness of the Albian/Cenomanian reservoir ranges from about 137 to 411.5 m. Petrographic analyses were conducted on two cores retrieved from the Albian/Cenomanian cycles covering the depth interval of 1323–1352 m in well AB-5. Most of the samples consist of quartz arenite and feldspathic arenite. The 3D facies model of the reservoir shows that the sandstone has a large probability distribution in the study area compared to the shale and siltstone. The 3D petrophysical models imply that the Albian/Cenomanian reservoir has good to very good reservoir quality. The main issue for the reservoir is the high water saturation values. In contrast, the hydrocarbon saturation is restricted to some parts of the basin.

**KEY WORDS:** Komombo Basin, Albian/Cenomanian, Sabaya/Maghrabi Formations, Reservoir characterization, 3D static model, Upper Egypt.

## INTRODUCTION

Petroleum companies and geologists consider that rift basins are the most important and primary targets for oil and gas exploration in North Africa (Nagati 1986; Meshref 1990; MacGregor et al. 1998; Bosworth et al. 2008). Aeromagnetic and gravity

data show elongated low structures in the southern part of the Western Desert, which are considered as half-graben basins (Klitzsch 1984; Wycisk 1987; Meshref 1990). According to Taha and Aziz (1998), the Komombo Basin (KB) in the Western Desert and the Nuqura and Kharit basins in the Eastern Desert are half grabens and defined as faulted rifts (Fig. 1). These grabens are not well studied, so their re-evaluation is necessary so as to provide much useful information about the hydrocarbon potential in these sedimentary basins (Ali et al. 2017b). The first published information about the petroleum presence in Upper Egypt was reported by Nagati

<sup>1</sup>Geology Department, Assiut University, Assiut, Egypt.

<sup>2</sup>DEA Company, Cairo, Egypt.

<sup>3</sup>Geology Department, Cairo University, Cairo, Egypt.

<sup>4</sup>To whom correspondence should be addressed; e-mail: moamen.mohamed@science.au.edu.eg

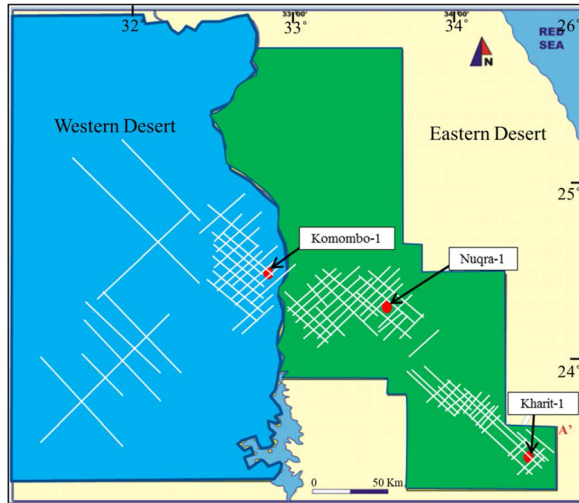


**Figure 1.** The Komombo, Nuqra and Kharit half-graben basins in Upper Egypt.

(1986). He discussed the presence of a triple junction in Upper Egypt. He also identified and pointed to the occurrence of the Mesozoic rift basins in Upper Egypt from the interpretation of the aeromagnetic data, namely Wadi Natash/Wadi Kharit to the east of the Nile and in the area between Edfu and Sin El Kadab to the west of the Nile.

The KB is situated in the southern Western Desert, about 65 km northwest of Aswan (Fig. 2a). It is considered a half graben (Fig. 3) and an intra-continental rift basin; it is the only producing basin in southern Egypt (Ali et al. 2017a). Bosworth et al. (2008) mentioned that the stress regime created in North and Central Africa associated with the opening of the South Atlantic was responsible for the formation of the KB. This basin is bounded by a major normal fault striking NW–SE that is situated on the NE side of the KB and downthrown to the southwest. There are also many minor normal faults that are characterized by the same NW–SE direction. The KB contains sediments (Fig. 4), about 4000 m thick, mainly clastics (shale and sandstone) with some carbonate deposits (Ziegler 1992). The KB holds two oil fields, Al Baraka and West Al Baraka fields (Fig. 2b), and it is a great exploration area for the GANOPE and DANA petroleum companies because most of the previous work and exploration activities until the 1990s concentrated on the unstable shelf in the northwestern desert where thick marine Cretaceous and Jurassic sediments were identified. Therefore, this study aimed at

a detailed study of the major structural elements and to discuss the characteristics of the main reservoirs of the KB, which have not been studied previously.

The Albian/Cenomanian reservoir is one of the two main reservoirs that contribute to the petroleum system in the KB (Ali 2017). These reservoirs have not been studied previously in detail. Therefore, the main objectives of the current research were to integrate 2D seismic reflection sections and wire-line logs, in addition to thin sections from core samples and descriptions of ditch samples, in order to (1) determine the main structural elements of the study area by constructing a depth structure contour map and 3D structure and horizon models, (2) perform petrographic study of the Albian/Cenomanian reservoir in well AB-5 through thin-section examination, (3) study the thickness variations and facies distribution of the Albian/Cenomanian reservoir by constructing an isochore contour map and a 3D facies model and (4) investigate the petrophysical characteristics of the reservoir and their distribution by conventional well log analyses and construction of 3D petrophysical models.

Studying the petrography of reservoir rocks using core thin sections has been applied by many authors (e.g., Hosseini et al. 2013; Dong et al. 2018; Nabawy et al. 2018; Jumat et al. 2018). Studying the structural, facies and petrophysical characteristics of reservoirs using 3D static modeling technique has been applied by many authors (e.g., Chihi et al. 2013; Adeoti et al. 2014; Abdel-Fattah and Tawfik 2015; El-Khadragy et al. 2017; Qadri et al. 2017; Abdel-Fattah et al. 2018; Eahsanul-Haque et al. 2018; Qadri et al. 2019; Abdelmaksoud et al. 2019a, b; Adelu et al. 2019; Barakat et al. 2019; Oyeyemi et al. 2019).

The main advantage of 3D modeling techniques is the ability to model complex structures. This technique allows the researcher to evaluate the model by viewing cross sections along any direction through the constructed model. The concept of 3D facies/petrophysics is also essential for linking well-bore measurements to a 3D static or geological model (Bryant and Flint 1993; Bilodeau et al. 2002; Cosentino 2005; De Jager and Pols 2006; Abdel-Fattah et al. 2010, 2018; Abdelmaksoud et al. 2019a, b; Abu Amarah et al. 2019).

## STRATIGRAPHY OF THE KOMOMBO BASIN

The stratigraphic column of the KB is representative of non-marine and shallow marine se-

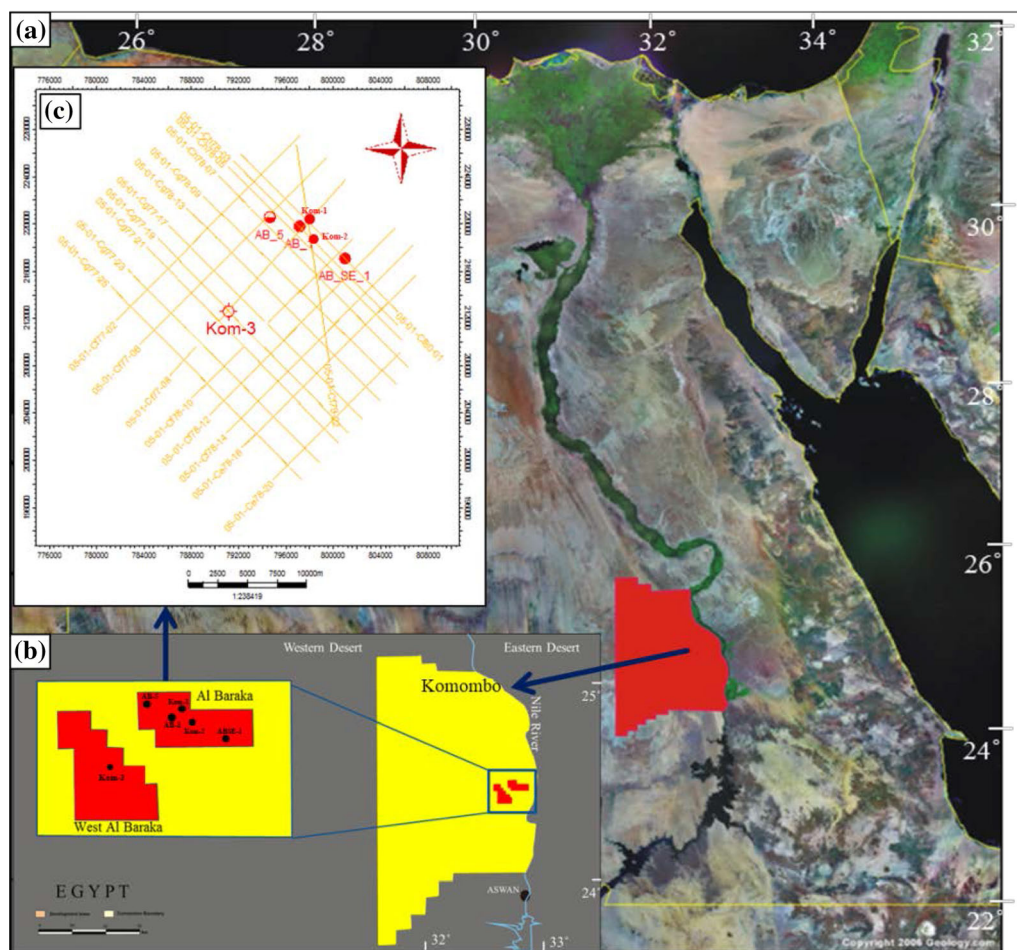


**Figure 2.** (a) Landsat image (MDA Federal 2004) showing the study area within Komombo basin, Southern Egypt (Ali et al. 2017b). (b) and (c) Base maps showing locations of the boreholes and 20 2D seismic lines used in this study.

quences deposited during the Cretaceous (Abdelhady et al. 2016). The stratigraphic succession is composed of seven formations: from top to bottom, the Dakhla, Qusier, Taref, Maghrabi, Sabaya, Abu Ballas and Six Hills Formations (Fig. 4). The Albian/Cenomanian (Sabaya/Maghrabi Formations) consists of shallow marine sands and shales. The cycle is commenced by coarse-grained siliciclastic quartzose sandstone with a general fining upward trend and silty and muddy facies at the top of the cycle (Abdelhady 2016). This cycle is divided into regressive and transgressive sub-cycles through the Albian and Cenomanian, respectively. In the Albian sub-cycle, above a sedimentary break (formation of a thick palaeosol), fluvial sandstone was deposited during Albian time due to recognizable eustatic or global sea-level fall. This interval consists mainly of

sandstone with shale and siltstone streaks. These sediments contain small species of Lamellibranchia des, gastropods, brachiopods, sea urchins, frequent fish and other vertebrate remains, as well as Middle Cretaceous flora. The sub-cycle is quite similar to the Bahariya Formation of the northern part of the Western Desert of Egypt (Dominik 1985). The Cenomanian sub-cycle represents a transgression phase above the Albian sequence of the regressive phase. The sediments are shallow marine facies composed of flaser-bedded siltstone and sandstone, in addition to shale with dolomite streaks in certain areas. Furthermore, palaeosol and fluvial sandstone intercalations are present. There is a gap in sedimentation and formation of topographic paleo-relief (Bisewski 1982). The thicknesses of the Albian/Cenomanian sequence vary in the drilled wells and



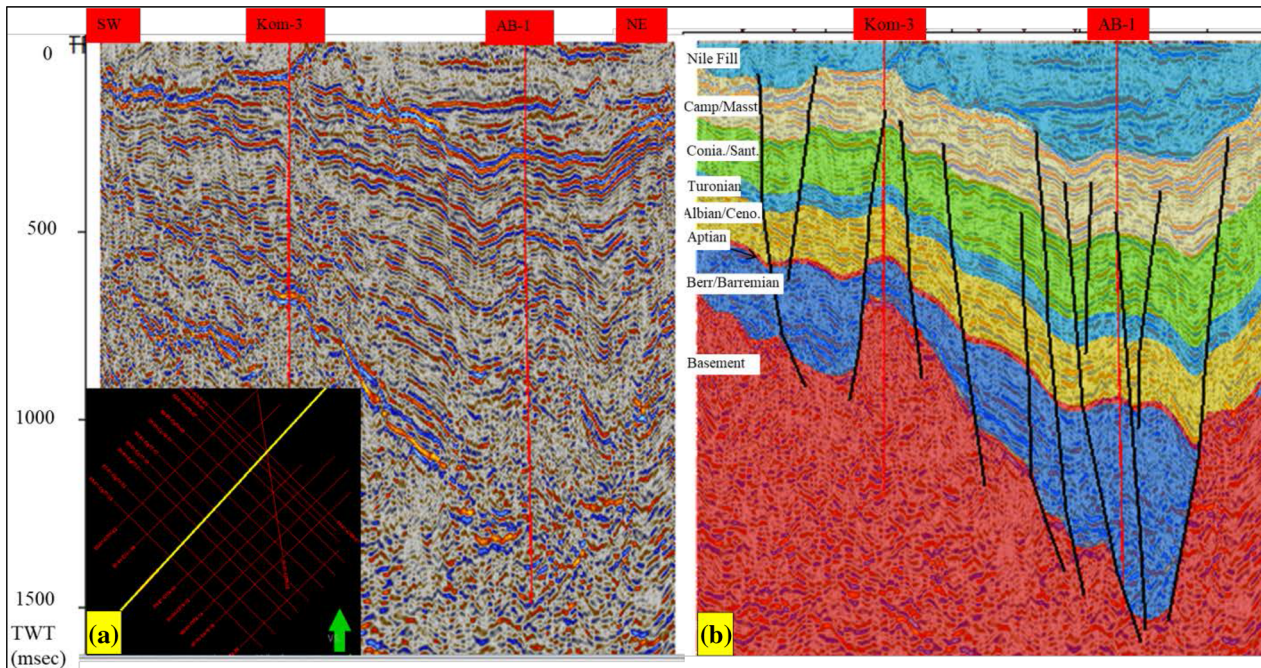


**Figure 3.** (a) Un-interpreted NE-SW 2D seismic section (05-01-Cf77-08) crossing the Komombo basin, Upper Egypt. (b) Interpreted NE-SW 2D seismic section showing the half-graben basin and the main seismic horizons in the study area.

are 221, 140.2, 302.4, 260, 411.8 and 292.6 m in the Kom-1, Kom-2, Kom-3, AB-1, ABSE-1 and AB-5 wells, respectively.

## DATABASE AND METHODS

The available data sets that were used for the present study include six well logs (Kom-1, Kom-2, Kom-3, AB-1, ABSE-1 and AB-5 wells), three vertical seismic profiles (VSPs), as well as 20 2D seismic lines; 12 of them have NW to NNW trends, and the other eight lines have NE trends (Fig. 2c). The available well log measurements are represented by gamma ray, caliper, neutron, density, sonic, shallow/deep resistivity and spontaneous potential logs. Additionally, the data sets include thin sections from core samples covering the depth interval of 4340–4436 ft (1323–1352 m) in well AB-5 and ditch sample descriptions of wells Kom-3, AB-1, ABSE-1 and AB-5. The available data were integrated into the Petrel™ Schlumberger modeling software for building a 3D structural/model for the Albian/Cenomanian reservoir. The interpretation of seismic data using Petrel™ involved tying seismic data to wells, interpreting faults and picking the Albian/Cenoma-

nian horizon to construct the two-way time (TWT) surface (Fig. 8). This surface was then converted to a depth structure surface using the velocity surface (Abdelmaksoud et al. 2017; Ali et al. 2017a, 2018). The velocity surface was generated by interpolating the velocity values at well locations. These values were obtained from the available time–depth relations within the VSPs. The results of the interpretation were used in the 3D structural modeling process as input data. This model represents the framework for the subsequent 3D facies and petrophysical models. The structural modeling comprised three main steps: fault modeling, pillar gridding and making horizons.

The first step in the construction of the 3D model was represented by the fault modeling process. This process represents the insertion of the interpreted faults into the structural model. These faults define breaks along the horizons, inserted later. The second process was pillar gridding. This process represents the generation of structural grids from the fault model. The third process was making horizons that represent the construction of the vertically stacked layers in the model by the insertion of the interpreted horizons. Through this process, the offsets on the faults were defined as well. The pro-



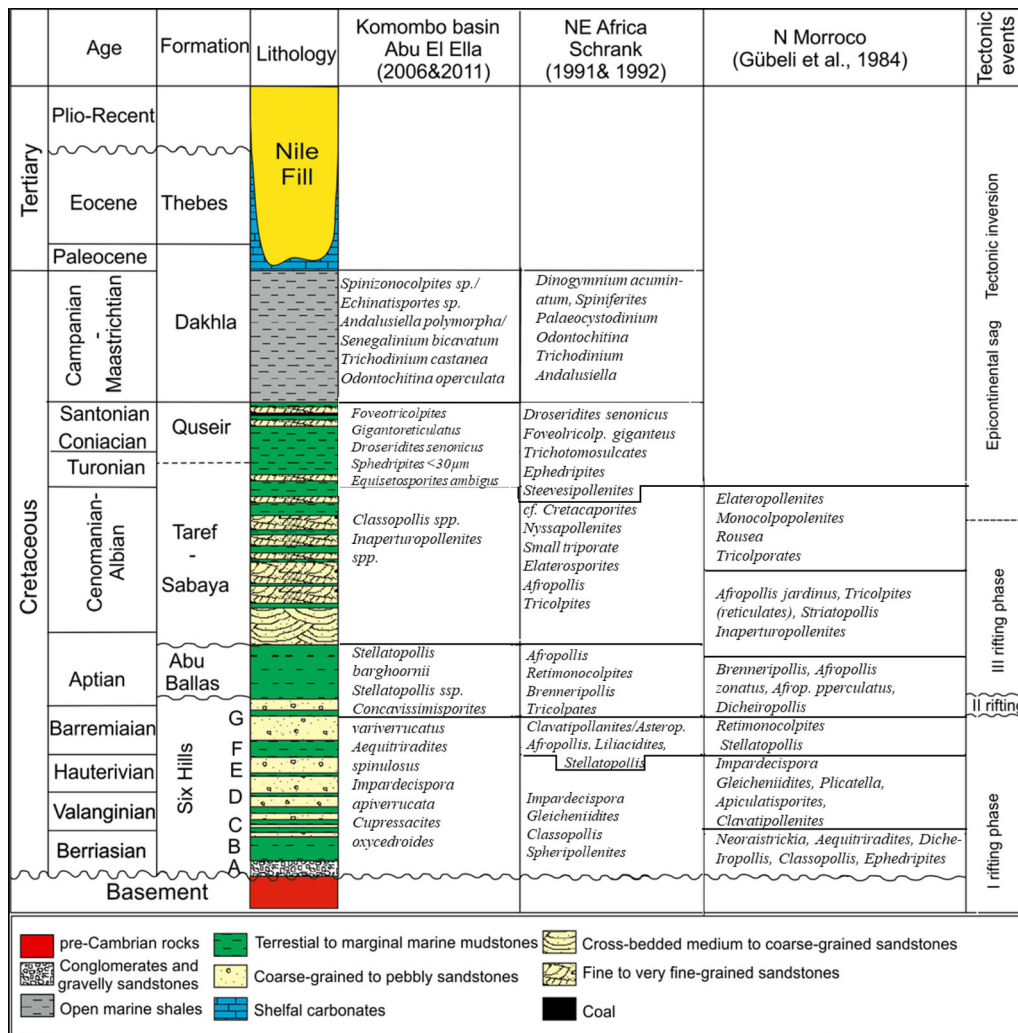


Figure 4. Stratigraphic chart of the Komombo Basin, showing that the stratigraphic succession is representative of non-marine and shallow marine deposits during the Cretaceous. (Selim 2016).

cess of making horizons generated independent geological horizons from XYZ input data (Cosentino 2005; Abdelmaksoud 2017; Abdelmaksoud et al. 2019b). These input data were the depth surfaces of the top and bottom of the Albian/Cenomanian reservoir. The purpose of the 3D structural model of the Albian/Cenomanian was to delineate and understand the structure and horizon setting of the reservoir in 3D patterns. The objective was to develop a reliable structural model of the field with only a few wells by maximizing the information from seismic data. The faults were modeled in 3D space and tied to the seismic horizons. The fault framework was quality checked with reference to the

interpreted 2D seismic maps. The 2D seismic interpretation provided grid data for the different horizons bounding the reservoir. The horizon seismic grid data were quality checked with reference to the well formation tops. Minor portions of grids for the different units showed inconsistencies with the well formation tops. These surfaces were re-gridded with a higher weighting factor on well formation tops from well logs inside the Petrel software. For the non-drilled area, the horizons were extended and extrapolated using the seismic data as a background.

The structural modeling was followed by analyses of the different conventional well logging curves for obtaining the various petrophysical char-

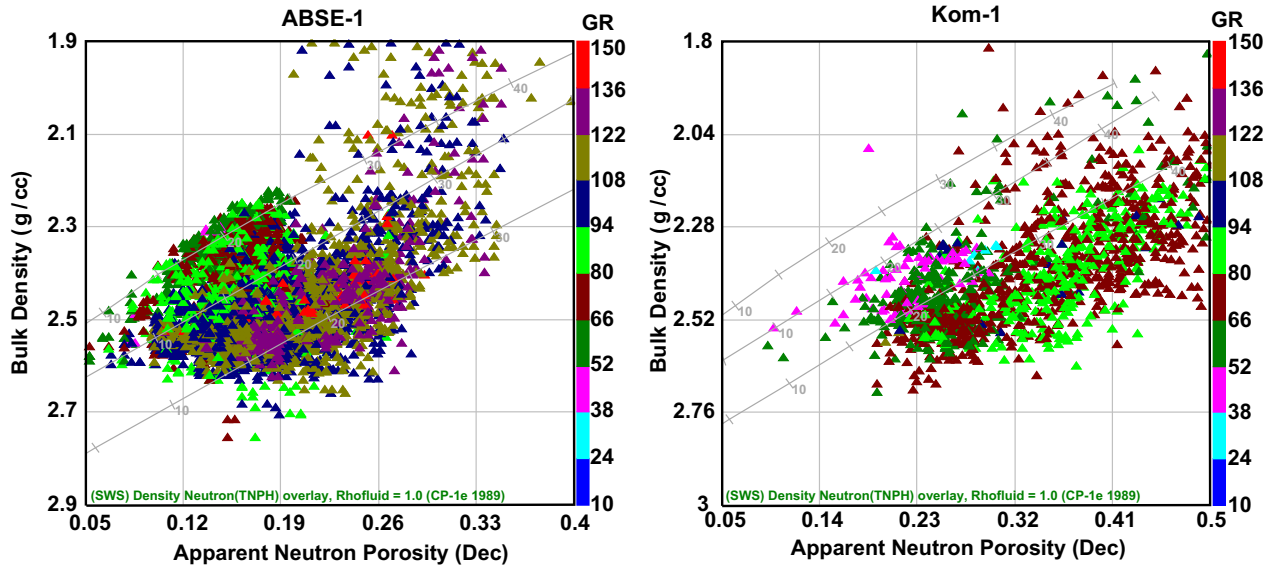


Figure 5. Neutron–density cross-plots of the Albian/Cenomanian reservoir (example of wells ABSE-1 and Kom-1) for identifying the comprising lithology.

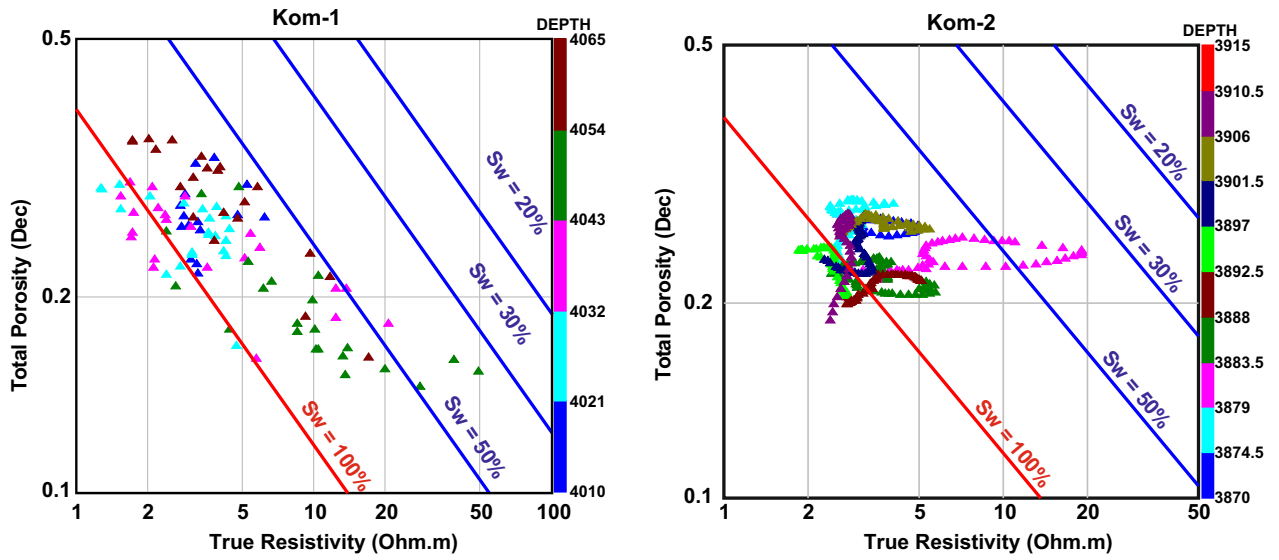


Figure 6. Cross-plot of deep resistivity ( $R_t$ ) vs. total porosity values ( $\phi$ ) (Pickett's plot) for the interval 3871.6–3911.4 ft (1180.1–1192.2 m) in Kom-2 well and the interval 4013.5–4064 ft (1223.3–1238.7 m) in Kom-1 well.

acteristics. The lithological interpretation of the Albian/Cenomanian reservoir was based on the investigation of the thin sections obtained from the core samples in addition to the different well logs, i.e., different well logs and neutron–density cross-plots (Fig. 5).

The water resistivity ( $R_w$ ) and cementation factor ( $m$ ) of the Albian/Cenomanian reservoir, which are needed for the saturation evaluation, were determined using the resistivity–porosity relationship of Pickett's plot (Pickett 1972). These values were 0.16 at the reservoir temperature (332.6°K) for  $R_w$  and 1.93 for  $m$  (Fig. 6). Cross-plotting of gamma

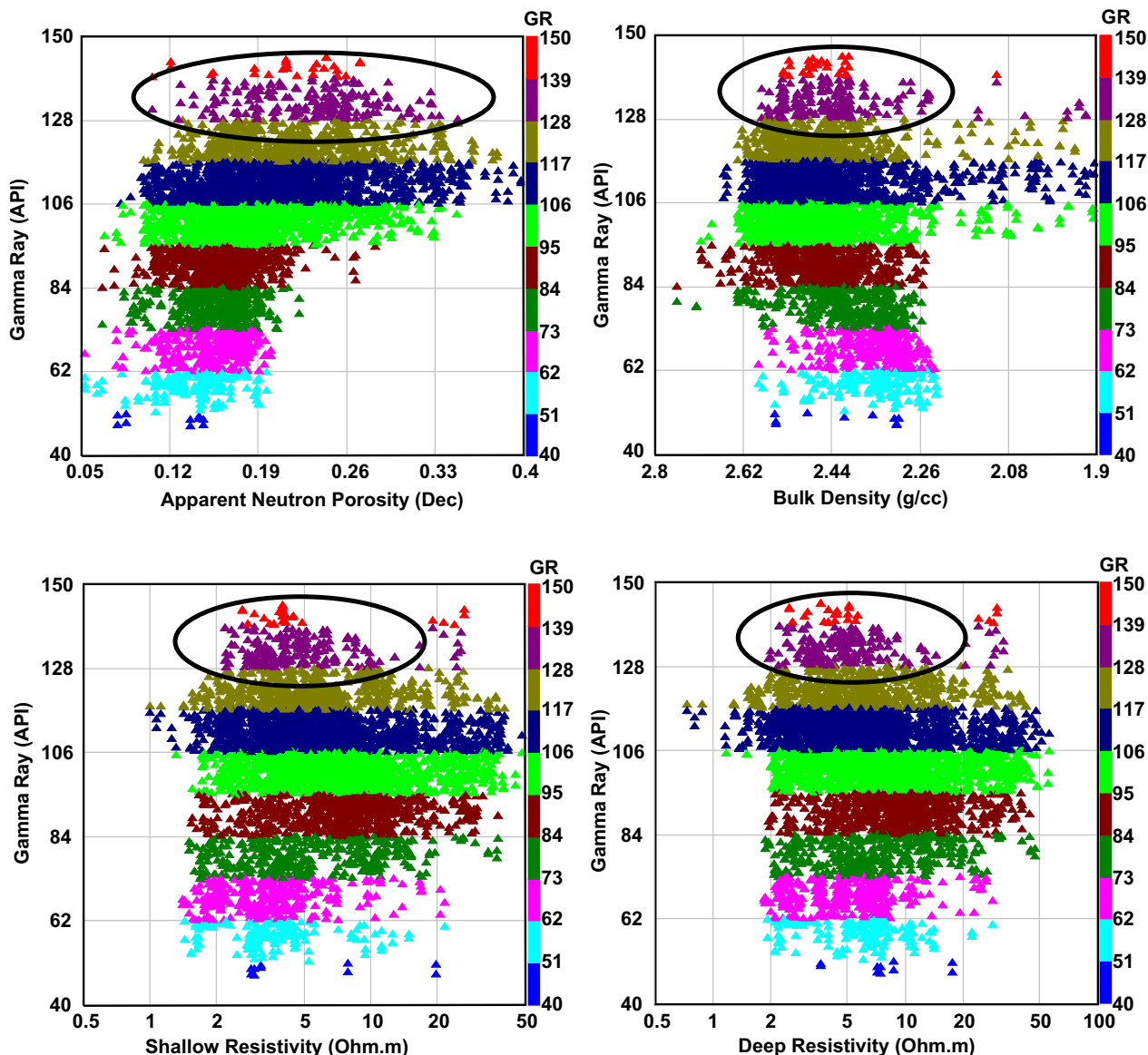


Figure 7. Cross-plots of bulk density, apparent neutron porosity, shallow resistivity and deep resistivity values vs. gamma ray values (example of ABSE-1 well). The black oval shape represents the pure shale lithology.

ray values vs. bulk density, apparent neutron porosity, shallow resistivity and deep resistivity values was used to obtain the shale parameters (Fig. 7 and Table 1). These parameters were represented by the resistivity of shale ( $R_{sh}$ ), neutron porosity of shale ( $\Phi N_{sh}$ ) and density of shale ( $\rho_{sh}$ ). In the Interactive Petrophysics™ software, the equation of Larionov (1969) for older rocks was used to calculate the clay volume ( $V_{cl}$ ). The total and effective porosities ( $\Phi_t$  and  $\Phi_e$ , respectively) of the studied

reservoir were calculated using the combination of neutron and density logs. The water saturation ( $S_w$ ) was calculated using the Indonesian equation (Popon and Leveau 1971) because the studied reservoir contains variable amounts of clay. The hydrocarbon saturation ( $S_{hc}$ ) was calculated by subtracting  $S_w$  from 100% saturation.

Permeability ( $K$ ) in the Albian/Cenomanian reservoir is known to be intermediate due to the variable clay content; therefore, the Timur equation



**Table 1.** Estimated shale parameters of the Albian/Cenomanian reservoir in the studied wells

Well	Parameter		
	$R_{sh}$ ( $\Omega$ m)	$\rho_{sh}$ (gm/cc)	$\Phi N_{sh}$ (%)
AB-5	3.50	2.40	34
ABSE-1	5.75	2.45	24
AB-1	3.50	2.30	29
Kom-1	5.00	2.39	34
Kom-2	4.90	2.40	31
Kom-3	12.0	2.32	37

(Timur 1968) was used to obtain an approximate value for permeability. Empirical estimates of permeability have uncertainties, but the Timur equation provides the lowest. The  $S_{wi}$  values were set to 0.01 below the lowest water saturation observed anywhere in the reservoir in logs (Darling 2005; Abdelmaksoud 2017; Abdelmaksoud et al. 2019a). Cutoff values were used to obtain the net reservoir and pay thicknesses. These values were 40% for shale volume, 10% for porosity and 60% for water saturation. The petrography of the reservoir rocks was investigated using polarizing microscopy. This investigation included the determination of the reservoir composition and the understanding of the

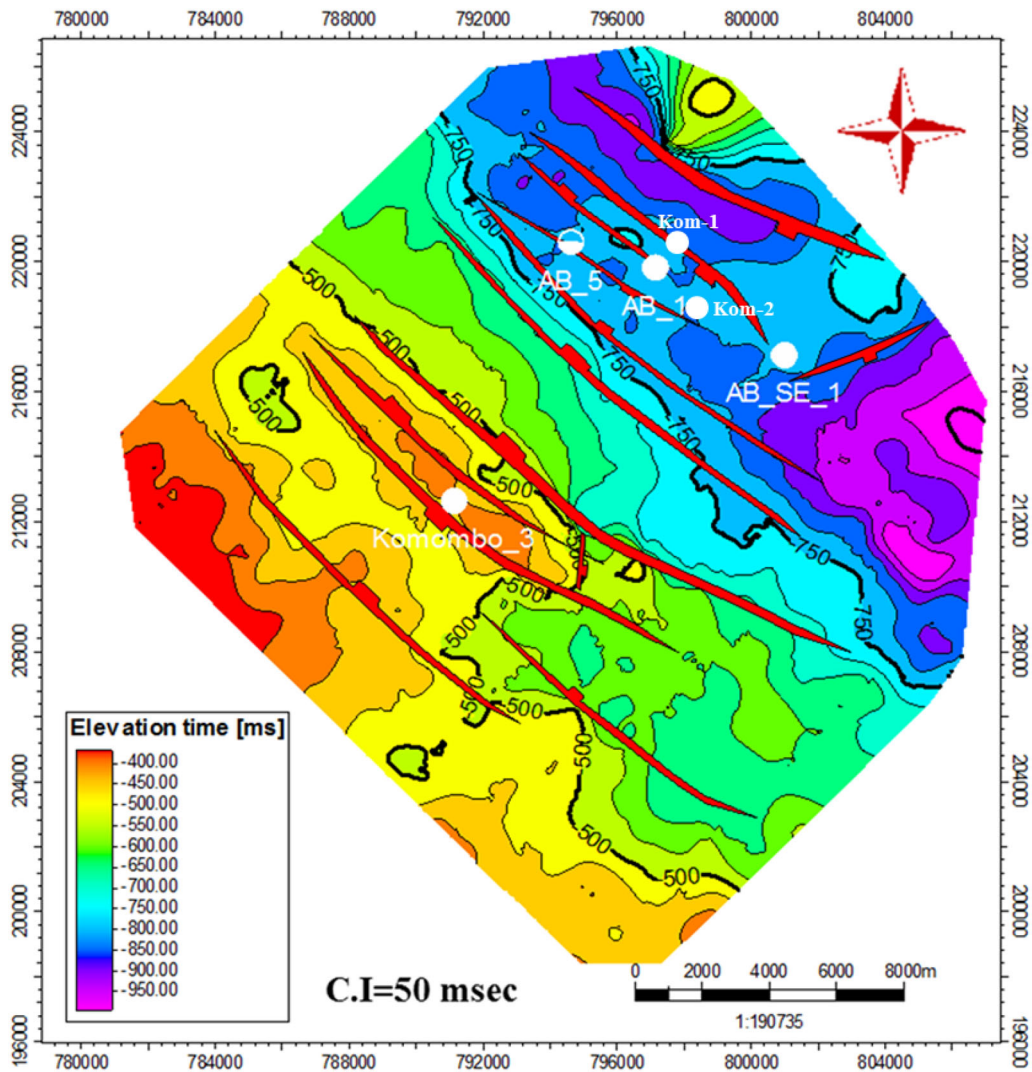


**Figure 8.** Two-way time contour map of the Albian/Cenomanian reservoir.

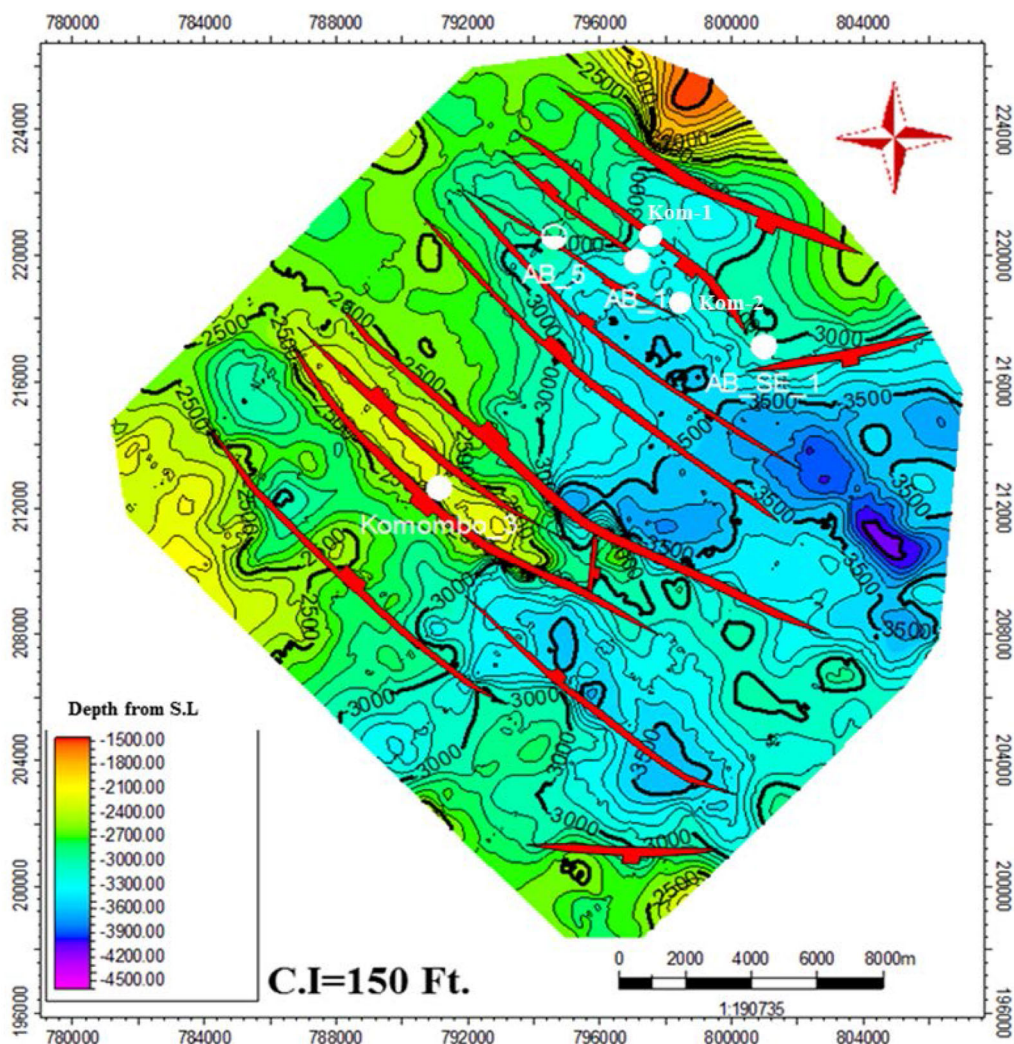


Figure 9. Depth (in ft) structure contour map of the Albian/Cenomanian reservoir (1 ft. = 0.3048 m).

relationship between the different authigenic minerals as well as the diagenetic features of the studied samples. The petrographic analyses were conducted on two cores retrieved from the Albian/Cenomanian cycles (Cores no. 1 and 2) covering the depth interval 4340–4436 ft (1323–1352 m) in well AB-5 and were performed through thin-section examination. The different interpreted lithologies/facies and petrophysical characteristics were then used as input in the constructed 3D structural framework through the processes of facies and petrophysical modeling in order to obtain 3D facies and petrophysical models for the studied reservoir.

## RESULTS AND DISCUSSION

### TWT Map of Top of the Albian/Cenomanian Reservoir

The TWT contour map of the top of the Albian/Cenomanian (Sabaya/Maghrabi formations) displays two main general normal fault trends in the NW–SE and NE–SW directions (Fig. 8). The TWTs of the reservoir increase in the eastern and north-western parts of the KB, recording maximum values of about 0.95 and 0.85 s, respectively, representing low structural features. The TWTs decrease in the southern and western parts of the KB, recording the

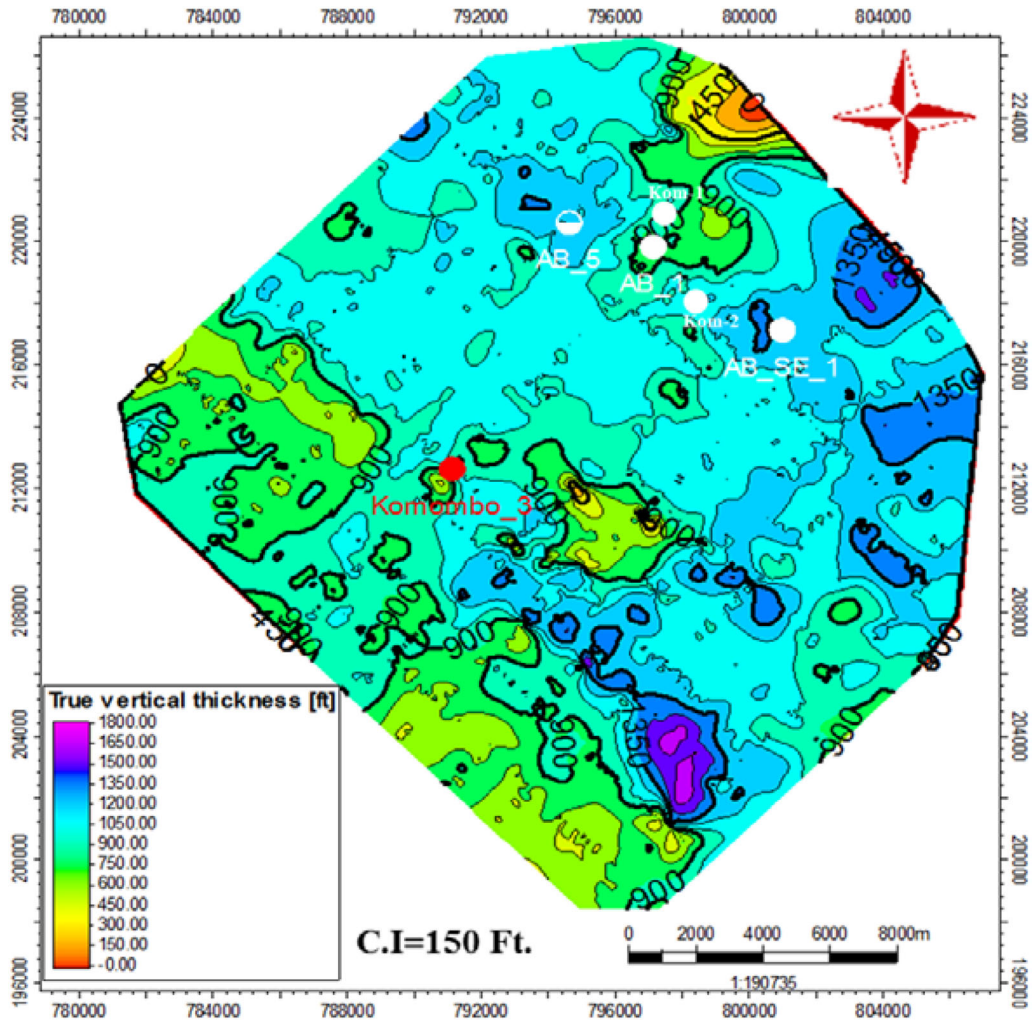


Figure 10. Isochore contour map of the Albian/Cenomanian reservoir (1 ft. = 0.3048 m).

minimum value of about 0.4 s representing high structural features.

**Depth Structure Contour Map of the Albian/Cenomanian Reservoir Top**

The depth structure contour map of the top of the Albian/Cenomanian reservoir shows that the KB is controlled by many normal faults. These faults form horsts and grabens due to tensional forces, so the displacements along these faults are reflected in the depth values of the reservoir. The maximum depth values are found in graben areas, and the minimum depth values are found in horst areas or at the shoulders of the basin. The depth values, as

deduced from the 2D seismic lines, range from between - 3000 and - 3950 ft (- 914 and - 1204 m) in the central and eastern parts (the depocenter of the basin) to between - 1500 and - 2000 ft (- 457 and - 610 m) in the western and northwestern parts of the KB (the shoulders of the basin) and to - 2200 ft (- 670.6 m) in the Komombo-3 well (horst) (Fig. 9).

**Isochore Map of the Albian/Cenomanian Reservoir**

The isochore map of the Albian/Cenomanian reservoir was constructed by subtracting the depth map of the Aptian interval from the depth map of the Albian/Cenomanian interval. Figure 10 shows



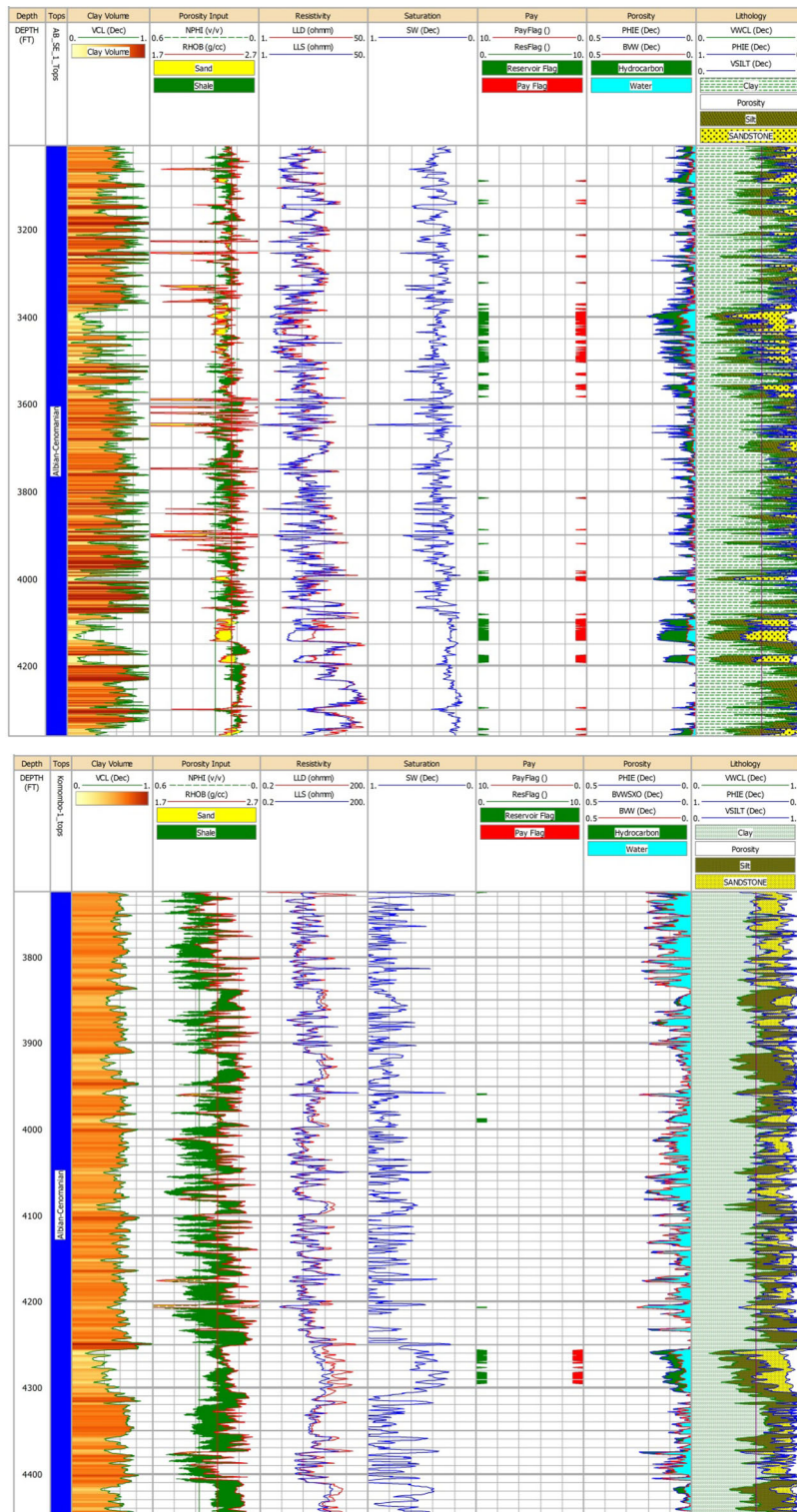


Figure 11. Litho-saturation cross-plots of the Albian/Cenomanian reservoir, example of ABSE-1 well (above) and Kom-1 well (below) (1 ft. = 0.3048 m).

**Table 2.** Averages of petrophysical parameters of the Albian/Cenomanian reservoir within the studied wells

Well	Gross thickness (m)	Net reservoir (m)	Net pay (m)	Net/gross	Average $\phi$ (%)	Average $V_{cl}$ (%)	Average $S_w$ (%)	Average $S_{hc}$ (%)	K (mD)
AB-5	292.49	22.33	3.12	0.076	14.90	26.20	70.20	29.80	0.5–625
ABSE-1	411.66	57.76	57.76	0.140	14.70	22.40	31.90	68.10	0.5–379
AB-1	260.1	44.96	21.64	0.173	22.20	16.60	55.90	44.10	0.5–1200
Kom-1	221	9.37	7.47	0.042	13.50	34.50	55.70	44.30	0.5–114
Kom-2	140.21	82.90	6.53	0.591	19.60	27.10	73.70	26.30	0.5–717
Kom-3	302.64	138.87	8.03	0.459	16.10	18.20	82.40	17.60	0.5–73.5

variable thickness of 450 ft (137.2 m) in the southern, western and central parts (due to the presence of the shoulders of the basin or horst structures). Meanwhile, the thickness of the reservoir in the eastern and southeastern parts of the KB ranges between 1000 and 1350 ft (304.8 and 411.5 m) due to the presence of the depocenter of the basin or graben structures. The large variation in the thickness of the reservoir may be related to the effect of the normal faults as the Albian/Cenomanian reservoir was deposited during the syn-rift stage (Selim 2016).

### Lithology and Petrophysical Parameters

The lithology of the Albian/Cenomanian reservoir is interpreted from well logs as sandstone cemented by argillaceous and/or calcareous materials, siltstone and shale. The obtained cross-plots exhibit three main clusters. The shale lithology is represented by the first cluster of these cross-plots, located in the upper part of the cross-plots. Shale is characterized by high gamma ray readings (100–130 API), high neutron porosity (24–37% porosity units, pu) and intermediate bulk density (2.30–2.45 g/cc), while deep resistivity is low (3.5–12  $\Omega$  m). The second cluster is located in the lower part of these cross-plots representing sandstone lithology. Sandstone exhibits by low gamma ray readings of about 30–40 API, low to intermediate neutron porosity (5–22% pu) and relatively intermediate bulk density (2.23–2.60 g/cc), while deep resistivity is relatively variable according to fluid content (2–200  $\Omega$  m). The third intermediate cluster represents the siltstone and shaly sandstone lithologies. Siltstone and shaly sandstone are characterized by intermediate gamma ray readings (40–100 API), variable neutron porosity due to variable clay content (5–35% pu), variable

bulk density (2.00–2.65 g/cc) and variable deep resistivity due to difference of fluid content (5–200  $\Omega$  m). The petrophysical parameters of the Albian/Cenomanian reservoir within the studied wells are presented in Fig. 11 and Table 2.

### Petrographic Aspects

Polarizing microscopy was used to investigate the petrography of reservoir rocks in order to determine their composition and to understand the relationship between the different authigenic minerals and the diagenetic features of the studied samples. The petrographic analyses were conducted on two cores retrieved from the Albian/Cenomanian cycles (Cores no. 1 and 2) covering the depth interval 4340–4436 ft (1323–1352 m) in well AB-5 and were performed through thin-section examination. Most of the samples consist of quartz arenite and feldspathic arenite. The quartz arenite with silt to coarse-grained sand has very poor reservoir quality and is poorly to moderately sorted, sub-angular to sub-rounded, moderately to highly cemented and moderately compacted. Feldspathic arenite also presents silt to medium-grained sand with poor reservoir quality and is moderately sorted, sub-angular to sub-rounded, highly to moderately cemented and strongly compacted with grain-to-grain contacts (Figs. 12 and 13).

### 3D Structural Model

The fault modeling of the Albian/Cenomanian sequence shows that the dominant fault system is represented by normal faults with NW–SE trends. Most of these faults are characterized by steep

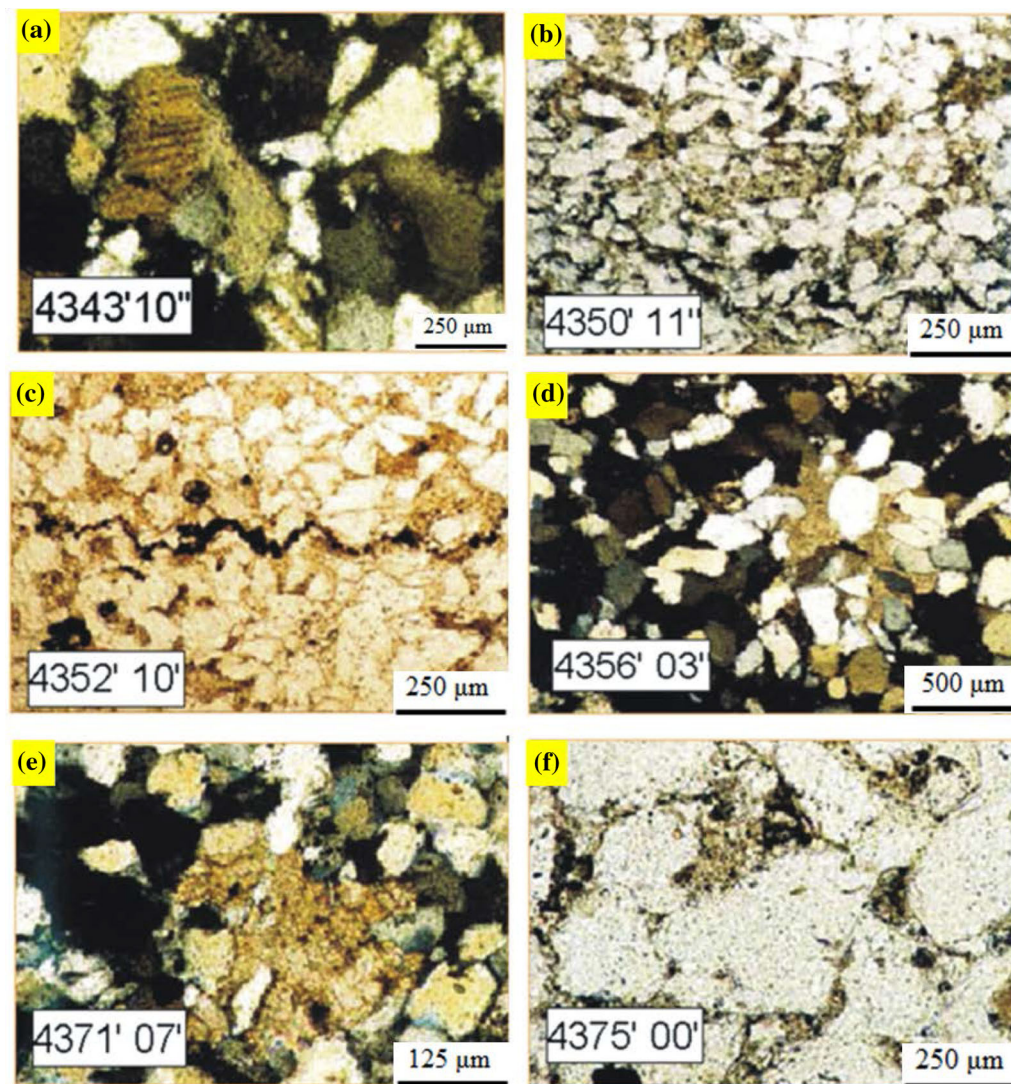


**Figure 12.** (a) Fine- to medium-grained arkosic sandstone, showing compaction resulting in concavo-convex and tangential contacts, poor visual porosity and permeability. (b) Fine-grained quartz arenite, showing compaction resulting in concavo-convex, long and tangential contacts, microstylolites, possible kerogen seams. (c) Fine-grained quartz arenite, showing compaction resulting in tangential and long contacts, poor porosity, microstylolites kerogen seams. (d) Fine- to medium-grained quartz arenite, showing compaction resulting in tangential contact, clay matrix and patchy calcite cement. (e) Siltstone, showing compaction resulting in concavo-convex and tangential contacts and calcite cement. (f) Fine- to medium-grained quartz arenite, showing compaction resulting in concavo-convex, tangential and long contacts and microstylolite. (1 ft. = 0.3048 m).

planes at the top parts with dip angles of  $60^{\circ}$  to  $80^{\circ}$ , while most of their lower parts have low to medium dip angles ( $20^{\circ}$  to  $40^{\circ}$ ) (Fig. 14). These faults are called listric or spoon faults. The amounts of displacement in most of these faults range between 40 and 200 ft (12 and 61 m) in the SE and NW directions, forming many horst, graben and half-graben structures. Some of these faults have large amounts of displacement ranging from 100 to 800 ft (30.5 to

244 m) (Fig. 15). The NW–SE and NE–SW trending normal faults resulted from the Early Cretaceous extension phase in the  $N35^{\circ}E$  and  $N45^{\circ}W$  directions, respectively, during the active opening of the south and equatorial Atlantic Ocean. This opening occurred during the Early Cretaceous rifting phases due to clockwise rotation of North and Central Africa, which was linked to the breakup of western Gondwana (Guiraud and Bellion 1995; Philobos



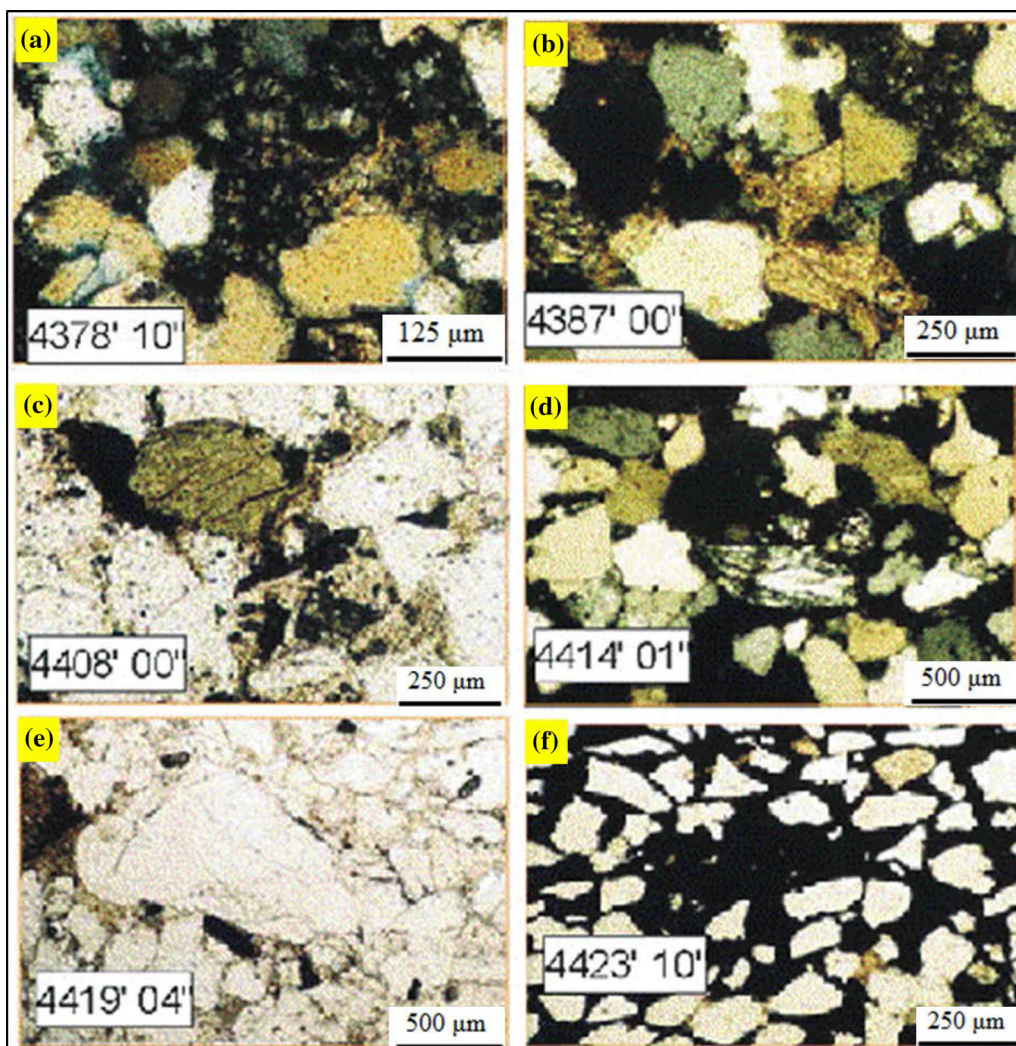


**Figure 13.** (a) Siltstone to fine-grained sandstone showing compaction resulting in concavo-convex and long contacts and kaolinite matrix. (b) Fine-grained sandstone, clay matrix, showing compaction resulting in concavo-convex and long contacts, euhedral carbonate spar cement. (c) Fine- to medium-grained sandstone, showing compaction resulting in concavo-convex, tangential and long contacts, rich in accessory minerals, clay matrix. (d) Fine- to medium-grained quartz arenite, showing compaction resulting in concavo-convex, tangential and long contacts, clay matrix. (e) Ill-sorted fine- to coarse-grained sandstone, showing high compaction resulting in concavo-convex, tangential and long contacts, altered feldspar and clay matrix. (f) Fine-grained quartz arenite, angular to sub-angular, with abundant iron oxides cement. (1 ft. = 0.3048 m).

et al. 2000; Noweir et al. 2002; Guiraud et al. 2005 and Bosworth et al. 2008). Figure 16 represents the 3D structural model of the Albian/Cenomanian reservoir and shows horizons that are dissected by many normal faults with NW–SE direction. Additionally, the figure shows that the depths of the Albian/Cenomanian reservoir have maximum values in the eastern and central parts of the KB and decrease gradually toward the corners of the basin.

### 3D Facies Model

The 3D facies model of the Albian/Cenomanian reservoir depends on the upscaling of the facies log for the available boreholes. The sequential indicator simulation (SIS) method in the Schlumberger Petrel software was selected to model the facies. The 3D facies model of the reservoir shows that the sandstone has a large probability distribution in the study area compared to the shale and siltstone (Fig. 17).

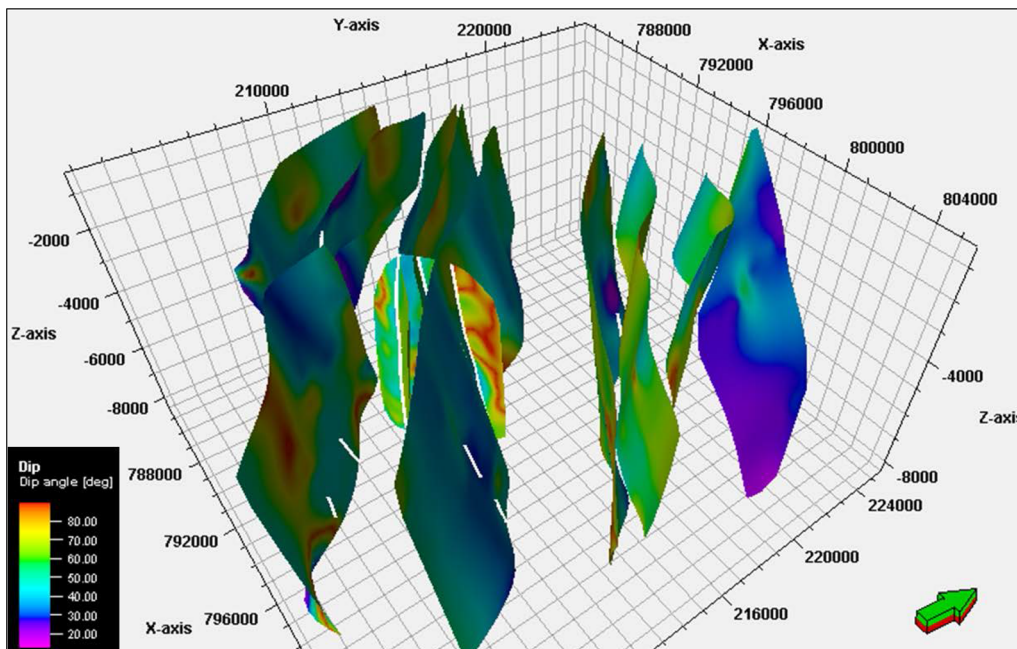


Figure 14. 3D fault model of the Komombo Basin showing the variation of dip angle of the normal faults. Units of X- and Y-axes are in meters and Z-axis in ft (1 ft. = 0.3048 m).

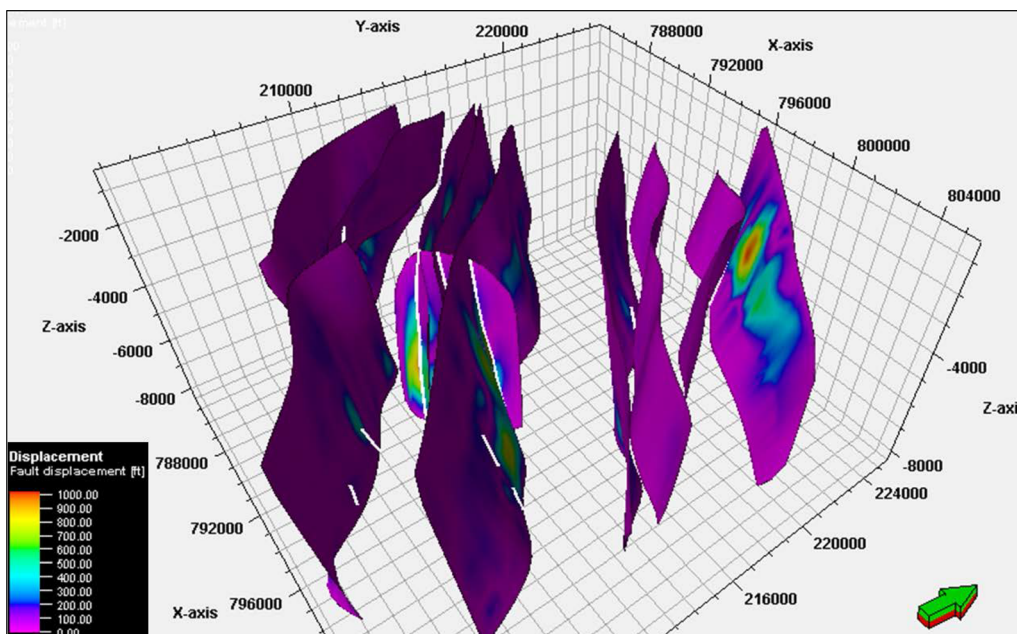
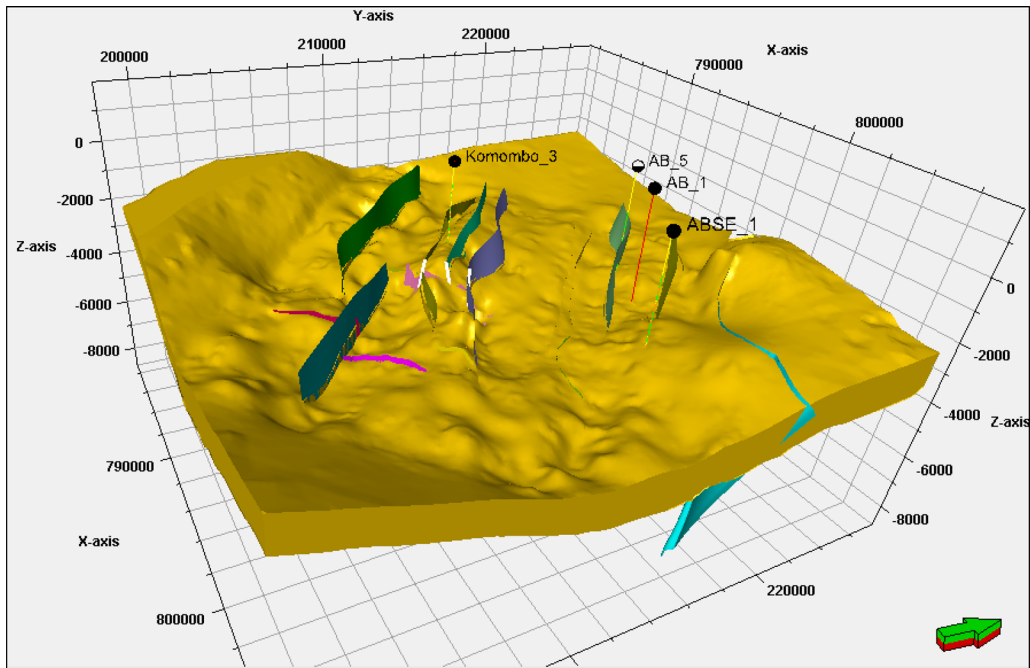
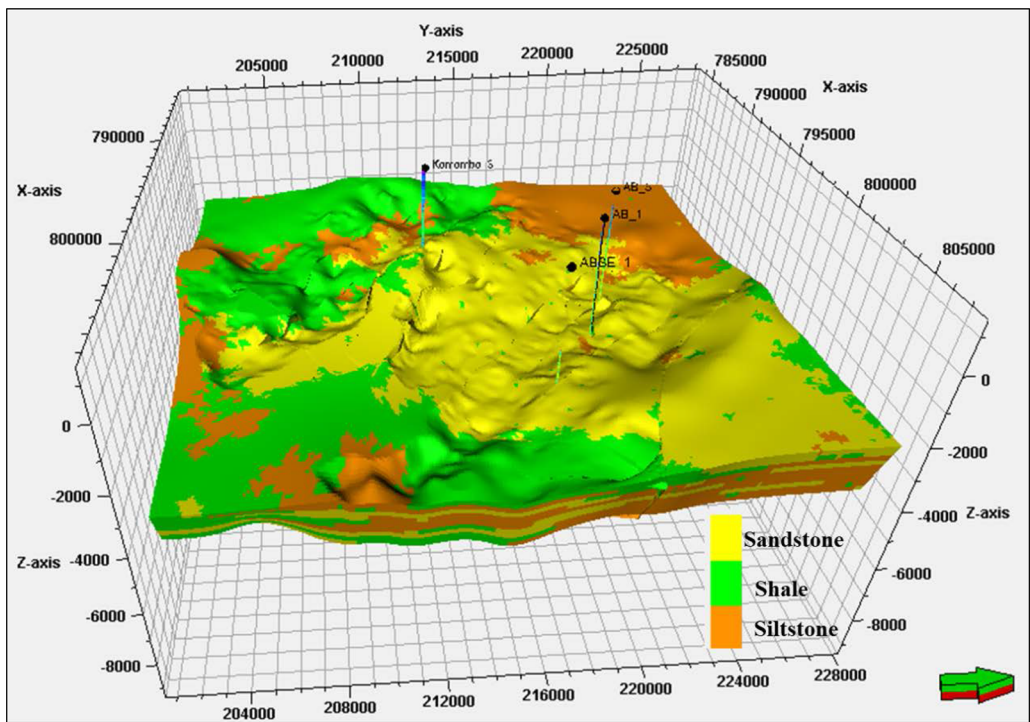


Figure 15. 3D fault model of the Komombo Basin showing the variation of displacements of the normal faults. Units of X- and Y-axes are in meters and Z-axis in ft (1 ft. = 0.3048 m).



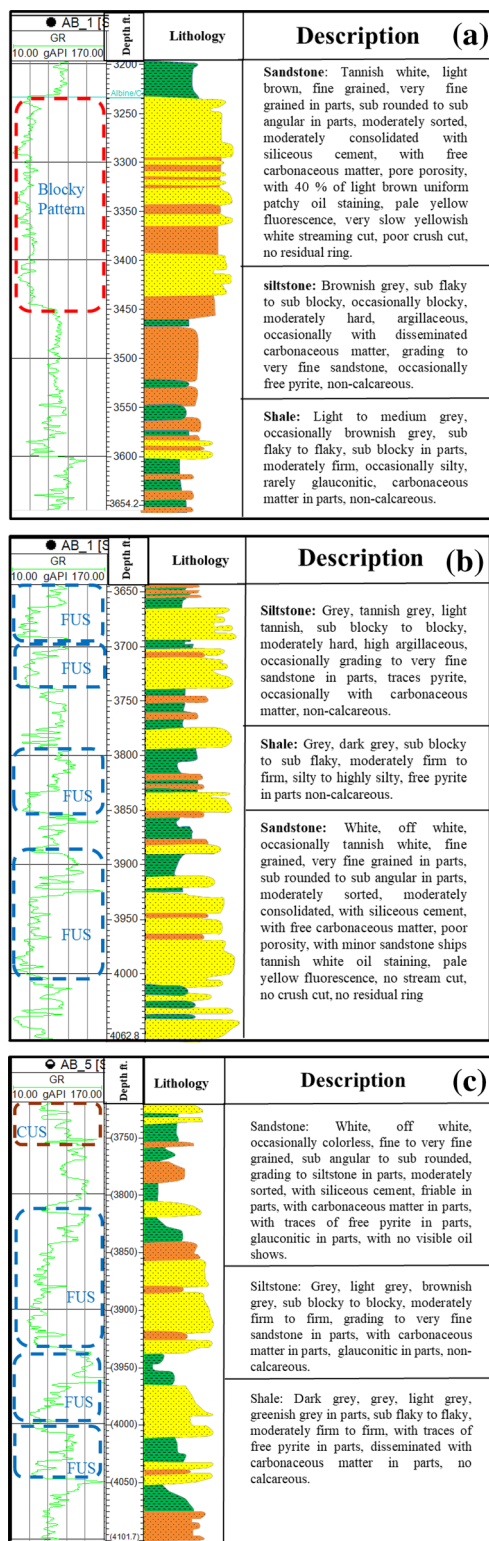


**Figure 16.** Albian/Cenomanian 3D reservoir structural model. Units of X- and Y-axes are in meters and Z-axis in ft (1 ft. = 0.3048 m).



**Figure 17.** 3D facies model showing the facies distribution of the Albian/Cenomanian reservoir. Units of X- and Y-axes are in meters and Z-axis in ft (1 ft. = 0.3048 m).





◀ **Figure 18.** Ditch samples' description and lithology of the Albian/Cenomanian section in AB-1 well, interval from: (a) 3650 to 3250 ft (1112.5 to 990.6 m). (b) 4060 to 3650 ft (1237.5 to 1112.5 m); (c) 3750 to 3400 ft (1143 to 1036.3 m). CUS = coarsening upward sequence; FUS = fining upward sequence.

The Albian/Cenomanian reservoir is composed mainly of about 45% sandstone with siltstone and shale at about 32% and 23%, respectively. The sandstone is concentrated in the central and north-eastern parts of the basin, while the siltstone is concentrated in the northwestern part. Most of the shale is distributed in the southeastern and southwestern parts of the KB (Fig. 17). The 3D facies model of the reservoir is consistent with the interpretation of depositional systems of the KB by Selim (2016). He proposed that the Albian/Cenomanian reservoir is represented by a fluvial-estuarine depositional system, consisting of many fining upward cycles that are composed mainly of fine- to medium-grained sandstone with thinly inter-bedded siltstones and mudstones that represent mixed-load fluvial channels. The description of the ditch samples and the patterns of the gamma ray logs of the six boreholes are consistent with this interpretation because the log patterns show attenuating blocky shapes and overall fining upward intervals with sand dominating the lower part of the depositional cycle and mudstones dominating the topmost part of the same cycle (Fig. 18a-c). Additionally, some top parts of the Albian/Cenomanian reservoir represent tidal channels and tidal bars. The tidal bar deposits show successive coarsening upward sequence (CUS), while the tidal channel is characterized by a fining upward sequence (FUS) (Fig. 18b and c).

Four cross sections were extracted from the 3D facies and structural models in the N-S, E-W, NE-SW and NW-SE directions, which display the detailed lithology and structural element configuration of the Albian/Cenomanian reservoir. The cross sections show large variations in the displacements of the normal faults 40 to 500 ft (12.2 to 152.4 m), forming many horst, graben and half-graben structures. The thickness of the Albian/Cenomanian reservoir increases in the graben and half-graben structures but decreases in the horst structures, which indicates syn-sedimentary tectonics (growth faults) (Fig. 19). Lateral and vertical facies changes through the studied reservoir were also noticed.

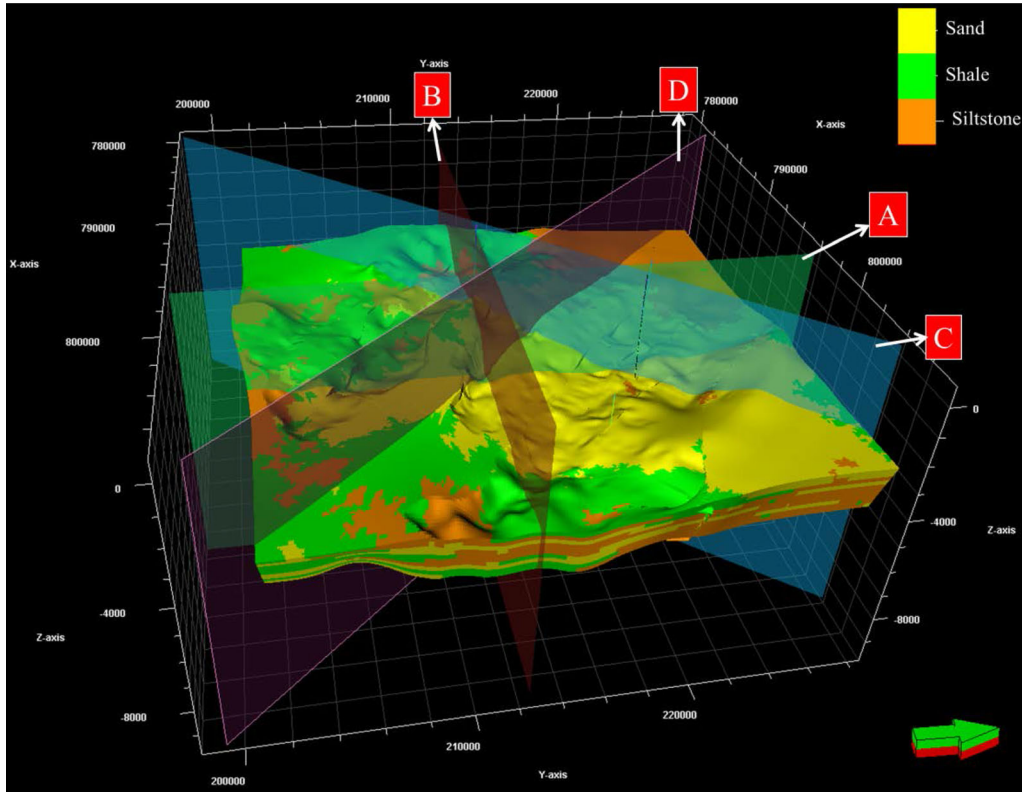


**Figure 19.** 3D facies and structural model in addition to the four extracted cross sections to displaying the detailed lithology and structure elements configuration of the Albian/Cenomanian reservoir. Units of X- and Y-axes are in meters and Z-axis in ft (1 ft. = 0.3048 m).

### 3D Petrophysical Model

The petrophysical parameters obtained from the Interactive Petrophysics™ software were up-scaled and then modeled using the petrophysical modeling process. The statistical method used in the petrophysical modeling process is the sequential Gaussian simulation algorithm. This method is appropriate, in the present case, given the amount of available data. The modeled parameters were porosity, permeability, water saturation and hydrocarbon saturation (Fig. 20). Some cross sections were extracted from these models to identify the 3D distribution of these parameters within the basin (Fig. 21).

The petrophysical models and the associated cross sections show that the Albian/Cenomanian reservoir is generally considered to have good to very good reservoir quality according to the classification of Etu-Efeotor (1997). This reservoir ex-

hibits generally medium to high porosity and permeability values. The reservoir also has medium to high water saturation values. Most of the Albian/Cenomanian reservoir within the KB has high water saturation values. In contrast, the hydrocarbon saturation is restricted to some parts within the basin. The porosity and permeability increase mainly in the central portion and toward the central eastern, central northern and southeastern portions of the study area, located within the main half graben of the basin and near the main fault that borders the basin on the northeast. The optimum hydrocarbon saturations through the studied reservoir generally increase in the central portion and toward the SE direction. AB-1 and ABSE-1 are considered hydrocarbon-bearing wells. Wells Kom-1, Kom-2, Kom-3 and AB-5 are considered water-bearing reservoirs because the net pay thicknesses for these wells are small.

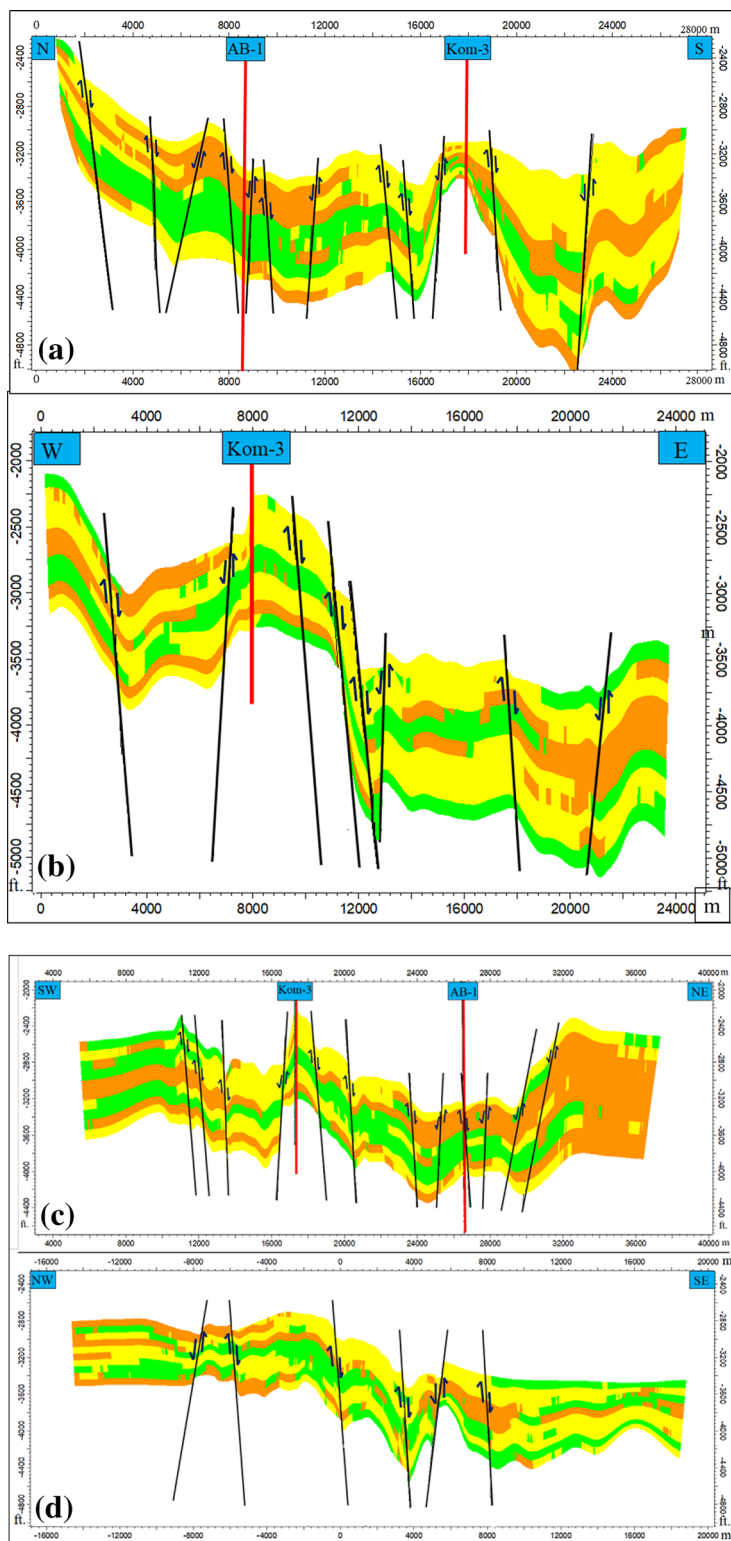
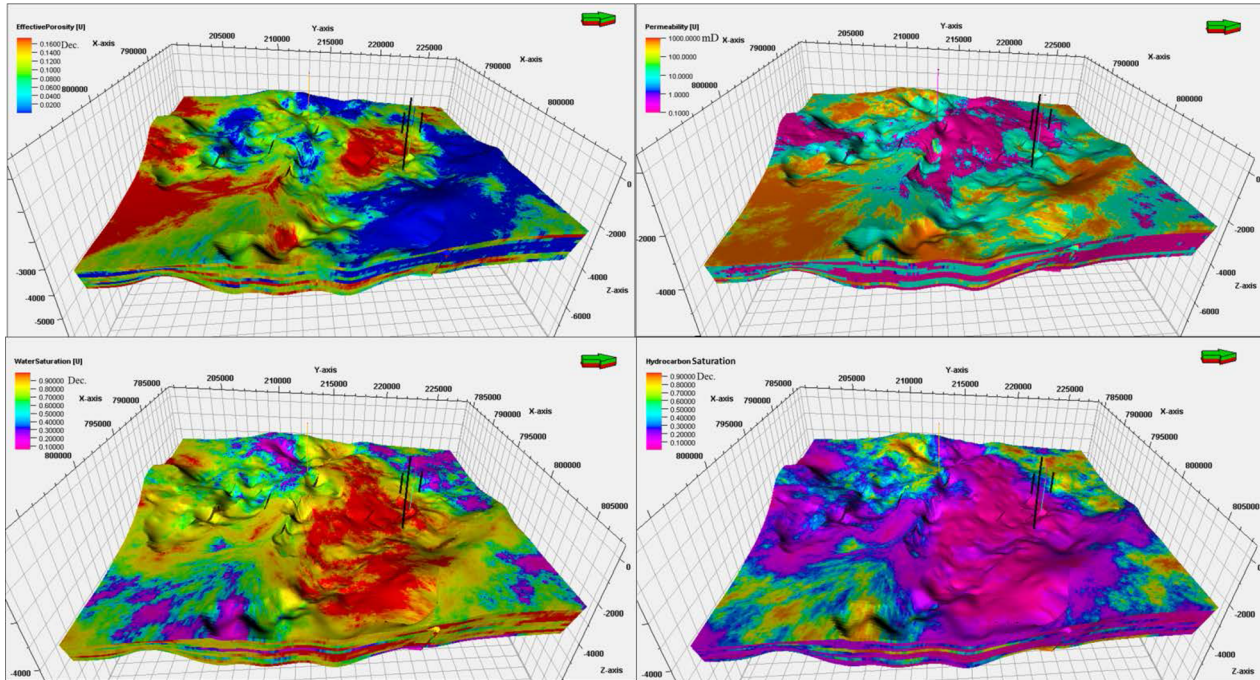


Figure 19. continued.





**Figure 20.** 3D views of the constructed petrophysical models, represented by porosity, permeability and water/hydrocarbon saturation. Units of *X*- and *Y*-axes are in meters and *Z*-axis in ft (1 ft. = 0.3048 m).

## CONCLUSIONS

The interpretation of the depth map shows two normal fault directions, NW–SE and NE–SW, where the NW–SE direction is dominant; the depth values range between  $-914$  and  $-1204$  m in the central and eastern parts and between  $-457$  and  $-610$  m in the western and northwestern parts of the KB. The thickness of the Albian/Cenomanian reservoir ranges from 137 to 411.5 m in the flanks and depocenter of the basin, respectively. The 3D fault modeling of the Albian/Cenomanian reservoir shows that most of the normal faults are characterized by steep planes in the upper parts with dip angles of  $60^\circ$  to  $80^\circ$ , while most of their lower parts have low to medium dip angles ( $20^\circ$  to  $40^\circ$ ). The amounts of displacement in most of these faults range between 12 and 61 m in the SE and NW directions, forming many horst, graben and half-graben structures. The 3D facies model shows that the Albian/Cenomanian reservoir is composed mainly of about 45% sandstone with siltstone and shale amounts of about 32% and 23%, respectively.

The petrographic analyses of the available core samples show that most of the samples consist of quartz arenite and feldspathic arenite. The 3D petrophysical models and the associated cross sections indicate good to very good quality for the reservoir, which has medium to high porosity and permeability. The main issue for the reservoir is the high water saturation values. In contrast, the hydrocarbon saturation is restricted to some parts of the basin. The porosity and permeability increase mainly in the central portion and toward the central eastern, central northern and southeastern portions of the study area, located within the main half graben of the basin and near the main fault that borders the basin in the northeast. The hydrocarbon saturations through the studied reservoir generally increase in the central portion and toward the SE direction. AB-1 and ABSE-1 are considered hydrocarbon-bearing wells. Wells Kom-1, Kom-2, Kom-3 and AB-5 are considered water-bearing reservoirs because the net pay thicknesses for these wells are small.

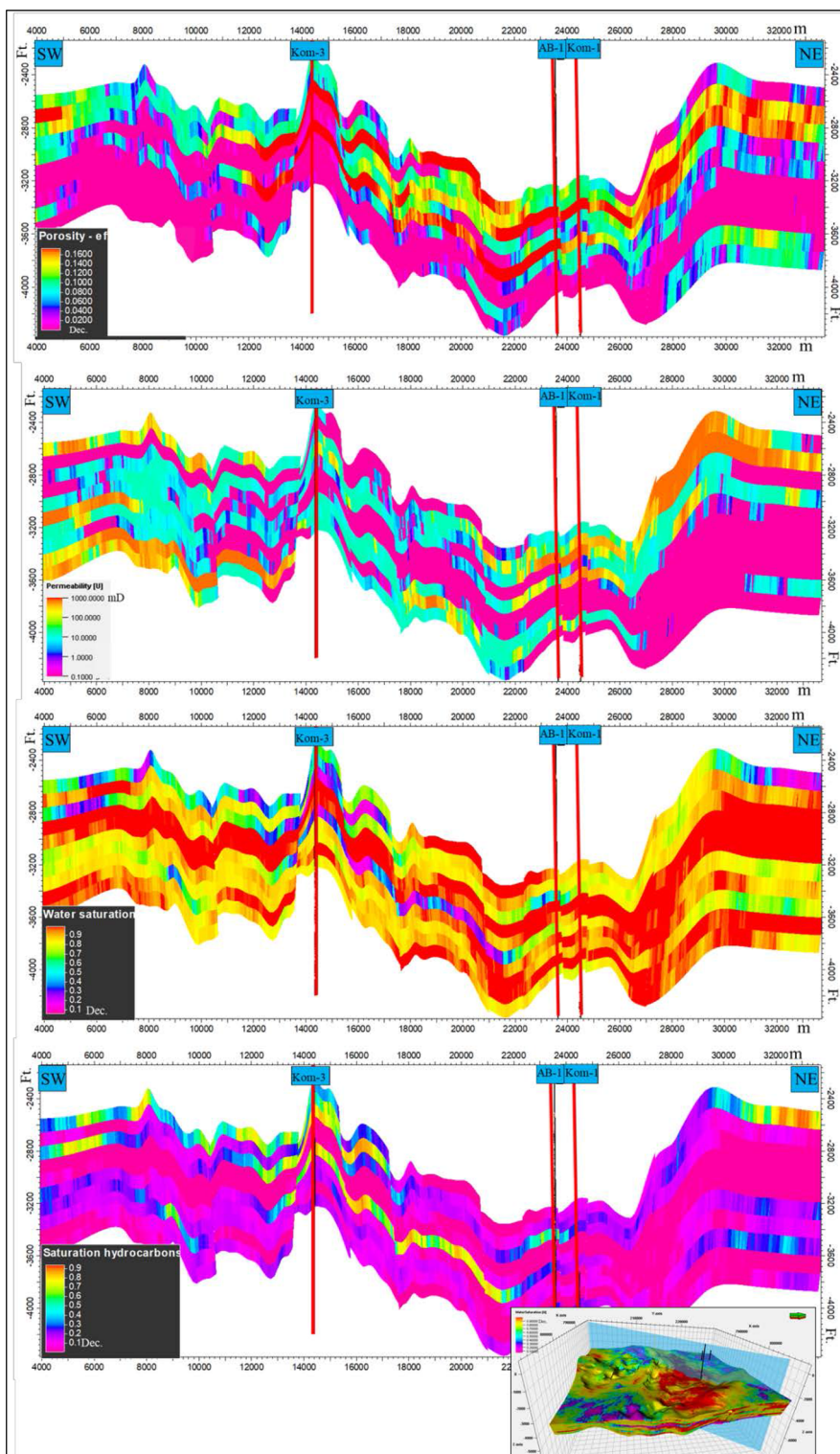


Figure 21. Cross sections through the different petrophysical models in NE-SW direction. Units of X-axis are in meters and Y-axis in ft (1 ft. = 0.3048 m).



## ACKNOWLEDGMENTS

The authors would like to acknowledge GANOPE Company for providing us with their seismic and well data and for giving us approval to publish our manuscript. The authors are grateful to Eng. Ahmed Samy (geophysicist at GANOPE) for fruitful discussion that led to a better understanding of many points. We would like to thank Ms. Nada Nabil (Commercial Project Manager, Nature Research Group, Springer Nature), Egyptian Knowledge Bank (EKB) and Eileen H. (Senior Editor, Springer Nature Author Services) for editing the manuscript for English language usage, grammar, spelling and punctuation by one or more native English-speaking editors at Nature Research Editing Service. Thanks are also due to the reviewers for their valuable comments and constructive modifications that greatly enhanced the manuscript. In addition, the authors would like to thank the Editor-in-Chief Prof. Dr. John Carranza for his effort in editing the manuscript.

## REFERENCES

- Abdel-Fattah, M., Dominik, W., Shendi, E., Gadallah, M., & Rashed, M. (2010). 3D integrated reservoir modelling for upper Safa gas development in Obaiyed field, Western Desert, Egypt. In *72nd EAGE conference and exhibition incorporating SPE EUROPEC, Spain*.
- Abdel-Fattah, M., Metwalli, F., & Mesilhi, E. (2018). Static reservoir modelling of the Bahariya reservoirs for the oil-fields development in South Umbarka area, Western Desert. *Egypt. Journal of African Earth Sciences*, *138*, 1–13.
- Abdel-Fattah, M., & Tawfik, A. Y. (2015). 3D geometric modeling of the Abu Madi reservoirs and its implication on the gas development in Baltim area (Offshore Nile Delta, Egypt). *International Journal of Geophysics*, *2015*, 1–11.
- Abdelhady, A. (2016). *Hydrocarbon potential and petroleum occurrence in Komombo sedimentary basin, South West Nile Valley, Upper Egypt*. Ph.D. Thesis, Faculty of Science, Cairo University, Egypt.
- Abdelhady, A., Darwish, M., El-Araby, A., & Hassouba, A. (2016). Evaluation of Neocomian shale source rock in Komombo basin, Upper Egypt. *IJISSET - International Journal of Innovative Science, Engineering & Technology*, *3*(1), 376–382.
- Abdelmaksoud, A. (2017). *Integrated geological modelling of the upper Bahariya reservoir in Abu Gharadig oil and gas field, North Western Desert, Egypt*. M.Sc. Thesis, Faculty of Science, Assiut University, Egypt.
- Abdelmaksoud, A., Amin, A. T., El-Habaak, G. H., & Ewida, H. F. (2019a). Facies and petrophysical modelling of the Upper Bahariya Member in Abu Gharadig oil and gas field, north Western Desert, Egypt. *Journal of African Earth Sciences*, *149*(C), 503–516.
- Abdelmaksoud, A., Ewida, H. F., El-Habaak, G. H., & Amin, A. T. (2017). Seismic interpretation of Abu Roash "G" member, in Abu Gharadig oil and gas field, north Western Desert, Egypt. *Journal of Basic and Environmental Sciences*, *4*(2), 107–117.
- Abdelmaksoud, A., Ewida, H. F., El-Habaak, G. H., & Amin, A. T. (2019b). 3D structural modelling of the Upper Bahariya Member in Abu Gharadig oil and gas field, North Western Desert. *Egypt. Journal of African Earth Sciences*, *150*(C), 685–700.
- Abu Amarah, B. A., Nabawy, B. S., Shehata, A. M., Kassem, O. M., & Ghrefat, H. (2019). Integrated geological and petrophysical characterization of Oligocene deep marine nonconventional poor to tight sandstone gas reservoir. *Marine and Petroleum Geology*. <https://doi.org/10.1016/j.marpetgeo.2019.06.037>.
- Abu El-Ella, N. (2006). *Biostratigraphy and lithostratigraphy of Komombo-1, Komombo-2, Komombo-3, Nuqra-1 and Kharit-1 Wells, Upper Egypt*. Earth Resources Exploration (EREX), Unpublished internal report, Cairo.
- Abu El-Ella, N. (2011). *Biostratigraphic studies for the Al Baraka oil field, Upper Egypt*. Earth Resources Exploration (EREX), Unpublished internal report, Cairo.
- Adelu, A. O., Aderemi, A. A., Akanji, A. O., Sanuade, O. A., Kaka, S. I., Afolabi, O., et al. (2019). Application of 3D static modeling for optimal reservoir characterization. *Journal of African Earth Sciences*, *152*, 184–196.
- Adeoti, L., Onyekachi, N., Olatinsu, O., Fatoba, J., & Bello, M. (2014). Static reservoir modeling using well log and 3-D seismic data in a KN field, offshore Niger Delta. *Nigeria. International Journal of Geosciences*, *5*(1), 93.
- Ali, M. (2017). *Tectonostratigraphy and petroleum system analysis of Al Baraka Oil Field, Komombo Basin, South Western Desert, Egypt*. M.Sc. Thesis, Faculty of Science, Assiut University, Egypt.
- Ali, M., Darwish, M., Abdelhady, A., & Essa, M. A. (2017a). Structural and lithostratigraphic evolution of Al Baraka Oil field, Komombo Basin, Upper Egypt as deduce from 2D seismic lines and well logging data. *Journal of Basic and Environmental Sciences*, *4*(2), 149–169.
- Ali, M., Darwish, M., Abdelhady, A., & Essa, M. A. (2017b). Case study of seismic interpretation in Al Baraka Oil Field, Komombo Basin, Upper Egypt. In *5th international conference for young scientist in basic and applied science, Assiut, Egypt.*
- Ali, M., Darwish, M., Essa, M. A., & Abdelhady, A. (2018). 2D Seismic Interpretation and characterization of the Hauterivian-Early Barremian Source Rock in Al Baraka Oil Field, Komombo Basin, Upper Egypt. *Journal of African Earth Sciences*, *139*, 113–119.
- Barakat, M. K., El-Gendy, N. H., & El-Bastawesy, M. A. (2019). Structural modeling of the Alam El-Bueib Formation in the jade oil field, Western Desert, Egypt. *Journal of African Earth Sciences*, *156*, 168–177.
- Bilodeau, B., De, G., Wild, T., Zhou, Q., & Wu, H. (2002). Integrating formation evaluation into earth modelling and 3D petrophysics. In *SPWLA 43rd annual logging symposium.*
- Bisewski, H. (1982). Zur Geologie des Dakhla-Beckens (Südwest-Ägypten): Sedimentologie und Geochemie der Nubischen Gruppe. *Berliner Geowissenschaftliche Abhandlungen*, *40*(A), 1–85.
- Bosworth, W., El-Hawat, A. S., Helgeson, D. A., & Burke, K. (2008). Cyrenaican "shock absorber" and associated inversion strain shadow in the collision zone of northeast Africa. *Geology*, *36*, 695–698.
- Bryant, I. D., & Flint, S. S. (1993). Quantitative clastic reservoir geological modelling: Problems and perspectives. In S. S. Flint & I. D. Bryant (Eds.), *The geological modelling of hydrocarbon reservoirs and outcrop analogues. International Association of Sedimentologists Special Publication* (Vol. 15, pp. 3–20). Hoboken: Wiley.



- Chih, H., Bedir, M., & Belayouni, H. (2013). Variogram identification aided by a structural framework for improved geometric modeling of faulted reservoirs: Jeffara Basin, Southeastern Tunisia. *Natural Resources Research*, 22(2), 139–161.
- Cosentino, L. (2005). Static reservoir study. In P. Barnaba (Ed.), *Encyclopaedia of hydrocarbons* (Vol. I, pp. 553–573). Italy: Marchesi Grafiche Editoriali S.p.a. [http://www.treccani.it/portale/OPENCMS/handle/404?exporturi=/export/sites/default/Portale/sito/altre\\_aree/Tecnologia\\_e\\_Scienze\\_applicate/enciclopedia/inglese/inglese\\_vol\\_1/idro\\_vol\\_I\\_I\\_XXXVI\\_eng3.pdf](http://www.treccani.it/portale/OPENCMS/handle/404?exporturi=/export/sites/default/Portale/sito/altre_aree/Tecnologia_e_Scienze_applicate/enciclopedia/inglese/inglese_vol_1/idro_vol_I_I_XXXVI_eng3.pdf).
- Darling, T. (2005). *Well logging and formation evaluation*. Amsterdam: Elsevier.
- De Jager, G., & Pols, R. W. (2006). A fresh look at integrated reservoir modelling software. *First Break*, 24, 75–81.
- Dominik, W. (1985). Stratigraphie und Sedimentologie (Geochemie, Schwermetallanalyse) der Oberkreide von Bahariya und ihre Korrelation zum Dakhla Becken (Wester Desert, Ägypten). *Berliner Geowissenschaftliche Abhandlungen*, 62(A), 1–173.
- Dong, S. P., Shalaby, M. R., & Islam, M. A. (2018). Integrated reservoir characterization study of the McKee Formation, Onshore Taranaki Basin, New Zealand. *Geosciences*, 8(4), 105.
- Eahsanul-Haque, A. K., Islam, M. A., Shalaby, M. R., & Sadeque, J. (2018). Integrated 3D facies modeling of the Mangahewa Formation, Maui Gas Field, Taranaki Basin, New Zealand. *Journal of Petroleum Exploration and Production Technology*, 8(4), 1017–1049.
- El-Khadragy, A. A., Eysa, E. A., Hashim, A., & Abdel-Kader, A. A. (2017). Reservoir characteristics and 3D static modelling of the Late Miocene Abu Madi Formation, onshore Nile Delta, Egypt. *Journal of African Earth Sciences*, 132, 99–108.
- Etu-Efeotor, J. (1997). *Fundamentals of petroleum geology* (p. 146). Port Harcourt: Paragraphics.
- Gübeli, A. A., Hochuli, P. A., & Wildi, W. (1984). Lower Cretaceous turbiditic sediments from the Rif chain (northern Morocco)—palynology, stratigraphy and palaeogeographic setting. *Geologische Rundschau*, 73(3), 1081–1114.
- Guiraud, R., & Bellion, Y. (1995). Late Carboniferous to recent geodynamic evolution of the West Gondwanian cratonic Tethyan margins. In A. Nairn, L. E. Ricou, B. Vrielynck, & J. Dercourt (Eds.), *The ocean basins and margins, the Tethys Ocean* (pp. 101–124). New York: Plenum Press.
- Guiraud, R., Bosworth, W., Thierry, J., & Delplanque, A. (2005). Phanerozoic geological evolution of Northern and Central Africa: An overview. *Journal of African Earth Sciences*, 43, 83–143.
- Hosseini, S. A., Lashgari, H., Choi, J. W., Nicot, J. P., Lu, J., & Hovorka, S. D. (2013). Static and dynamic reservoir modeling for geological CO<sub>2</sub> sequestration at Cranfield, Mississippi, USA. *International Journal of Greenhouse Gas Control*, 18, 449–462.
- Jumat, N., Shalaby, M. R., & Islam, M. A. (2018). Integrated reservoir characterization of the Paleocene Farewell Formation, Taranaki Basin, New Zealand, using petrophysical and petrographical analyses. *Journal of Petroleum Exploration and Production Technology*, 8(3), 685–701.
- Klitzsch, E. (1984). Flora and fauna from strata in southern Egypt and northern Sudan (Nubia and surrounding areas). *Berliner Geowissenschaftliche Abhandlungen*, 50(A), 47–79.
- Larionov, V. (1969). *Borehole radiometry*. Nedra, Moscow.
- MacGregor, D. S., Moody, R. T. J., & Clark-Lowes, D. D. (1998). *Petroleum geology of North Africa* (Vol. 132). London: Geological Society London, Special Publication.
- MDA Federal. (2004). *Landsat GeoCover ETM+2000 Edition Mosaics*. Sioux Falls, South Dakota, USGS, Tiles: N-35-20, N-35-25, N-35-30, N-36-20, N-36-25 and N-36-30. ETM-EarthSat MrSID.
- Meshref, W. M. (1990). Tectonic framework. In R. Said (Ed.), *The geology of Egypt* (pp. 113–156). Rotterdam: A.A. Balkema.
- Nabawy, B. S., Rashed, M. A., Mansour, A. S., & Afify, W. S. (2018). Petrophysical and microfacies analysis as a tool for reservoir rock typing and modeling: Rudeis Formation, offshore October Oil Field, Sinai. *Marine and Petroleum Geology*, 97, 260–276.
- Nagati, M. (1986). Possible Mesozoic rift in Upper Egypt: An analogy with the geology of Yemen-Somalia rift basins. In *4th exploration and production conference, EGPC, Cairo, Egypt.*
- Noweir, A. M., Noweir, A. S., Nassm, A. S., Lebda, E. M., & El-Kholify, E. M. (2002). Late Cretaceous transpression—Tertiary extension affecting the Phanerozoic sedimentary formations, east KomOmbo south Eastern Desert, Egypt. *Middle East Research Center, Ain Shams University, Earth Science Series.*, 16, 145–165.
- Oyeyemi, K. D., Olowokere, M. T., & Aizebeokhai, A. P. (2019). Prospect analysis and hydrocarbon reservoir volume estimation in an exploration field, shallow offshore depobelt, Western Niger Delta, Nigeria. *Natural Resources Research*, 28(1), 173–185.
- Philobos, E., Riad, S., Omran, A. A., & Othman, A. B. (2000). Stages of fracture development controlling the evolution of the Nile Valley in Egypt. *Egyptian Journal of Geology*, 44, 503–532.
- Pickett, G. R. (1972). *Practical formation evaluation*. Golden Colorado: GR Pickett Inc.
- Poupon, A., & Leveaux, J. (1971). Evaluation of water saturation in shaly formations. In *Proceedings of the SPWLA 12th annual logging symposium*.
- Qadri, S. M. T., Islam, M. A., & Shalaby, M. R. (2019). Three-dimensional petrophysical modelling and volumetric analysis to model the reservoir potential of the Kupe Field, Taranaki Basin, New Zealand. *Natural Resources Research*, 28(2), 369–392.
- Qadri, S. M. T., Islam, M. A., Shalaby, M. R., & Eahsanul-Haque, A. K. (2017). Seismic interpretation and structural modelling of Kupe field, Taranaki Basin, New Zealand. *Arabian Journal of Geosciences*, 10, 295.
- Schrank, E. (1991). Mesozoic palynology and continental sediments in NE Africa (Egypt and Sudan)—A review. *Journal of African Earth Sciences*, 12, 363–373.
- Schrank, E. (1992). Nonmarine Cretaceous correlations in Egypt and northern Sudan: Palynological and palaeobotanical evidence. *Cretaceous Research*, 13, 351–368.
- Selim, S. S. (2016). A new tectono-sedimentary model for Cretaceous mixed nonmarine–marine oil-prone Komombo Rift, South Egypt. *International Journal of Earth Sciences*, 105(5), 1387–1415.
- Taha, M. A., & Aziz, H. (1998). Mesozoic rifting in Upper Egypt Concession. In *14th international petroleum conference, (abstract)*.
- Timur, A. (1968). An investigation of permeability, porosity and residual water saturation relationships for sandstone reservoirs. In *SPWLA 9th annual logging symposium, New Orleans, Louisiana* (Vol. 9, No. 4).
- Wycisk, P. (1987). Contribution to the subsurface geology of the Misaha trough and the southern Dakhla basin (S. Egypt/N. Sudan). *Berliner Geowissenschaftliche Abhandlungen*, 75(A), 137–150.
- Ziegler, P. A. (1992). Geodynamics of rifting and implications for hydrocarbon habitat. *Tectonophysics*, 215, 221–253.